The Effects of Entangled IR-Radiation and Tunneling on the Conformational Interconversion of 2-Cyanophenol

A. J. Lopes Jesus,[a,b,]* Cláudio M. Nunes,[a] I. Reva,[a] Sandra M. V. Pinto,[a,c] and R. Fausto[a]

[a] CQC, Department of Chemistry, University of Coimbra, 3004-535, Coimbra, Portugal.

[b] CQC, Faculty of Pharmacy, University of Coimbra, 3004-295, Coimbra, Portugal.

[c] Scuola Normale Superiore, Piazza dei Cavalieri, 7, I-56124 Pisa, Italy.

Abstract

The conformers of 2-cyanophenol (2CP) and their interconversions were studied by infrared spectroscopy after trapping monomers of the gaseous compound into low-temperature (15 K) argon (Ar) and nitrogen (N_2) matrixes. To assist in the interpretation of the experimental results, B3LYP, MP2 and QCISD electronic structure calculations were carried out for the 2CP molecule. Two planar conformers, *cis* and *trans* (orientation of OH with respect to the cyano group), are predicted with gas-phase populations at the sublimation temperature of ~ 98 % and ~ 2 %, respectively. The most stable form (*cis*) was experimentally identified in both cryomatrixes, whereas the less stable one (*trans*) was not detected in argon, but could be observed in the N_2 matrix with an abundance of ~15 %. Selective and bidirectional conversion between the two identified conformers was achieved upon irradiating the compound trapped in N_2 matrix with NIR laser light tuned at the wavenumbers of the 2ν(OH) transitions of the respective conformers. The conformational composition of 2CP was also found to be affected by the broadband infrared (IR) radiation emitted by the spectrometer source. This effect could be suppressed, partially or completely, by using different longpass infrared filters, with cutoff values near 2200, 1590, and 1170 cm^{-1}. The observed conformational changes are rationalized in terms of a competition between the over the barrier (light-induced) and through the barrier (hydrogen atom tunneling) effects. Very interestingly, both effects occur on a time scale of the same order.

* Corresponding author: A. J. Lopes Jesus

E-mail address: ajorge@ff.uc.pt

1. INTRODUCTION

2-Cyanophenol (2CP) is a phenol derivative substituted at the *ortho* position by a cyano group (−C≡N) (Chart 1). In this molecule, two distinct and stable orientations are possible for the OH group, which are commonly called *cis* or *trans*, depending if the OH is pointing towards the substituent or away from it, respectively.[1-3] Crystallographic,[4] thermochemical[5] and spectroscopic[2, 3, 6-10] studies have been performed on 2CP. Especially relevant for its conformational characterization were the results obtained by laser-induced fluorescence excitation spectroscopy of jet-cooled molecules[2, 9] and microwave spectroscopy of the gaseous compound.[3] In those studies, the low energy conformer (*cis*) was spectroscopically characterized, while the *trans* conformer was not detected because of its low abundance in gas phase. Moreover, only the *cis* form was identified in a low-temperature argon matrix when 2CP was generated by UV irradiation of 1,2-benzisoxazole.[11]

Matrix-isolation infrared spectroscopy, combined with methodologies that allow to manipulate the relative abundance of the conformers, is a suitable experimental tool for characterizing the conformational structure of molecules.[12, 13] One of such methodologies consists in applying near-IR (NIR) or mid-IR monochromatic radiation to excite selectively a vibrational mode of a specific conformer to generate another conformer(s).[14-18] In several cases, this resulted in the generation of a high-energy conformer,[19-21] which would otherwise be experimentally inaccessible. NIR excitation of first OH stretching overtones (2νOH) has been successfully used to promote conformational changes involving the torsional motion of OH groups, for instance in carboxylic acids,[21-24] alcohols,[17] aminoacids,[25-27] and nucleic acid bases.[28, 29] In most of these reported studies, the OH group is connected to a non-aromatic core. NIR induced rotamerizations of an OH directly connected to an aromatic ring have been only observed for cytosine,[30] 5-substituted cytosines,[28] and gallic acid.[31]

Modifications of the conformational distribution of matrix-isolated species can also result from the broadband IR radiation emitted by the light source of the spectrometer (globar). In fact, since the pioneering work of Hall and Pimentel,[15] who observed the isomerization of nitrous acid induced by the broadband IR light emitted by the spectrometer, this effect has been observed for various molecular systems.[28, 29, 32-34] Additionally, thermally induced processes, as well as quantum tunneling of light hydrogen atoms, can also promote conformational isomerizations. The latter effect has been previously observed for molecules having conformers differing from each other by internal rotation of an O−H group.[20, 21, 26, 27, 30, 35-39] In the present work, we demonstrate a rare case where the conformational dynamics of

an OH group is affected by the globar IR radiation and by hydrogen tunneling, both operating on the time scale of the experiment.

2. EXPERIMENTAL SECTION

A commercial sample of 2CP (Sigma-Aldrich, 99% purity), gaseous nitrogen (Air Liquide, N50) and argon (Air Liquide, N60) were used in the experiments. To prepare a low-temperature solid matrix, a small amount of solid 2CP was placed inside of a miniature glass recipient, connected to the vacuum chamber of a closed-cycle helium cryostat (APD Cryogenics, with a DE-202A expander). A gate valve was used so the path between the cryostat and the recipient (kept at ~ 298 K) could be closed once the deposition of the sample was finished, thus preventing further condensation of 2CP vapors on top of the matrix. Vapours of the compound were co-deposited with an excess of the matrix host gas (N_2 or Ar) onto a CsI optical substrate, cooled to15 K. The temperature of the CsI window was measured directly at the sample holder with an accuracy of 0.1 K by using a silicon diode sensor connected to a digital controller (Scientific Instruments, Model 9650-1). The process of the matrix deposition, which took approximately 2 hours, was controlled in real time by collecting IR spectra. For this purpose, the cold optical window of the cryostat was permanently placed in the spectrometer beam. IR spectra, both in the mid-IR (4000−400 cm^{-1}) and NIR (7500–4000 cm^{-1}) regions, were measured with a Thermo Nicolet 6700 Fourier-transform infrared (FTIR) spectrometer. In the mid-IR region, the spectra were recorded with a 0.5 cm^{-1} resolution using a deuterated triglycine sulphate (DTGS) or a liquid nitrogen-cooled mercury cadmium telluride (MCT/B) detector, together with a KBr beam splitter. In the NIR region, the spectra were recorded with 1 cm^{-1} resolution using the MCT/B detector and a CaF_2 beam splitter.

Monochromatic NIR radiation provided by the idler beam of a Quanta-Ray MOPO-SL optical parametric oscillator (OPO), pumped by a pulsed Nd:YAG laser, was employed to irradiate the deposited samples through the outer quartz window of the cryostat. The pulse duration and repetition rate were 10 ns and 10 Hz, respectively. The sample exposure to the IR light emitted from the source of the FTIR spectrometer (ETC EverGlo, globar), which provides energy within the 7400−50 cm^{-1} range in normal mid-IR operation mode, was also investigated. In some experiments, to partially protect the matrixes from the broadband radiation of the spectrometer, longpass filters, blocking IR light with wavenumbers above ~ 2200 cm^{-1} (Edmund Optics), ~ 1590 cm^{-1} (Spectrogon), or ~1170

cm^{-1} (Spectrogon), were used. To block all the broadband IR light (dark conditions) a metal plate was placed between the source of the spectrometer and the sample. A single beam spectrum collected with the spectrometer globar and transmittance spectra of the three used filters are provided as supporting information (Figure S1).

3. COMPUTATIONAL SECTION

All quantum-mechanical calculations were carried out with the Gaussian 09 program package (Revision D.01).[40] Geometries of the *cis* and *trans* conformers of 2CP were fully optimized using the B3LYP,[41-43] MP2 [44] and QCISD[45] electronic structure methods, combined, respectively, with the 6-311++G(d,p), 6-311++G(3df,3pd) and 6-31++G(d,p) basis sets. The Cartesian coordinates of the geometries optimized at the three levels are provided as supporting information (Table S1). B3LYP and MP2 harmonic vibrational calculations were performed on the geometries optimized at the respective levels. The Gibbs free energies extracted from these calculations were used to estimate the Boltzmann populations of two conformers at 298.15 K. The B3LYP harmonic wavenumbers (scaled by 0.950 and 0.980, above and below 3200 cm^{-1}, respectively) and respective IR intensities were used to simulate the IR spectra of the two conformers in the mid-IR region. The spectral simulations were performed with the Chemcraft software (version 1.8),[46] using Lorentzian functions with a full width at half maximum (FWHM) of 2 cm^{-1} and setting the intensity at the band maximum equal to the calculated IR intensity as taken from the Gaussian output. The normal modes of the two 2CP conformers were analysed by means of potential energy distribution (PED) calculations. The set of internal coordinates used in the PED analysis is given in Table S2 and the atom numbering is presented in Figure S2. In order to obtain the wavenumbers and IR intensities of the first overtones of the OH stretching vibrations, anharmonic vibrational calculations were carried out at the B3LYP/6-311++G(d,p) level, using the fully automated second-order vibrational perturbative approach developed by Barone and co-workers.[47, 48] The results of these calculations for the overtone transitions are given in Table S3. To elucidate some structural features of the 2CP conformers, a Natural Bond Orbital (NBO) analysis was performed using the NBO 3.1 program[49] implemented in Gaussian 09.

4. RESULTS AND DISCUSSION

4.1. Relative stability of the 2CP conformers

The energies computed for the *cis* and *trans* conformers of 2CP using three different electronic structure models show that *cis* is the most stable form (Table 1). The relative electronic energy (ΔE_{el}) of the *trans* conformer is 10.3, 9.9 and 8.3 kJ mol^{-1} at the B3LYP, MP2 and QCISD levels of theory, respectively. The QCISD energy difference is similar to that calculated at the CCSD(T)/6-311++G(d,p) level on geometries optimized at the MP2/6-311++G(d,p) level (7.9 kJ mol^{-1}).[3] Accounting for the contribution of the zero-point vibrational energy and of the thermal and entropic corrections at 298.15 K, the Gibbs energy difference (ΔG) between the two conformers amounts to 9.4 and 9.3 kJ mol^{-1} at the B3LYP and MP2 levels, respectively (Table 1). Applying a Boltzmann statistics, the equilibrium populations at 298.15 K for the *cis* and *trans* conformers are estimated to be ~ 98 % and ~ 2 %, respectively. Such a low abundance of the *trans* conformer might explain why this form was not experimentally detected in previous works.[2, 3, 9]

Figure 1 displays the geometries of the two conformers optimized at the QCISD level. The greater stability of the *cis* conformer is explained by the formation of a weak O−H···N≡C intramolecular hydrogen bond-like interaction[2, 3, 5, 6, 9, 50] [H···N = 2.78 Å ; O−H···N = 135.4°], which is not present in the *trans* conformer. This interaction is electronically manifested by the existence of πCN→σ*OH and σOH→π*CN donor-acceptor orbital interactions. The sum of the corresponding second-order perturbation energies, obtained from NBO calculations performed at the QCISD level, amounts to −7.3 kJ mol^{-1}. Other indication of this stabilizing interaction is the slight increase of the positive natural charge at the hydrogen atom (H_8), accompanied by a slight decrease of the negative charge at the nitrogen atom, when comparing *cis* with the *trans* conformer (Figure 1). The formation of the weak O−H···N≡C interaction is also supported by the spectroscopic observation of a 43 cm^{-1} red-shift in the OH stretching frequency of the *cis* conformer relative to the *trans* conformer, as shown in the next section.

Besides of the relative stability of the conformers, it is also interesting to estimate the height of the energy barrier separating the two conformers. The energy profile around the H−O−C1−C2 torsional angle was calculated at the B3LYP level (Figure 2). The computed energy barrier for the *cis* ↔ *trans* isomerization is 25 kJ mol^{-1} in the forward direction and 15 kJ mol^{-1} in the reverse direction. Accordingly, thermally induced processes are not supposed to alter the conformational distribution either in Ar or N_2 matrixes at a temperature as low as 15 K.[12, 51, 52]

4.2. Mid-IR Spectrum of 2CP isolated in Ar and N_2 matrixes

The experimental mid-IR spectra of 2CP monomers isolated Ar and N_2 matrixes, recorded immediately after finishing the process of the matrix deposition, are shown in Figures 3a and 3b, respectively. To assist in the assignment of the experimental bands, the B3LYP computed IR spectra of the *cis* and *trans* conformers are shown in Figure 3c. Table 2 lists the positions of the observed experimental bands, which are compared with the wavenumbers and IR intensities computed for both conformers. This table also includes a description of the vibrational modes based on the PED analysis.

The most intense bands in the Ar/N_2 matrixes spectra are observed at 3576/3572, 1491/1492 and 1214/1218 cm^{-1}. These bands match well the strongest IR absorptions computed for the *cis* conformer at 3580 [ν(OH)], 1482 [δ(CH)] and 1218 cm^{-1} [δ(COH)], respectively, thereby indicating that *cis* is, as expected, the dominant conformer of 2CP in both matrixes. Regarding the *trans* conformer, it was not detected in the Ar matrix, which, at first sight, is consistent with the theoretical predictions. For example, the strong IR absorption computed at 3641 cm^{-1} for the *trans* conformer [ν(OH), I = 87.2 km mol^{-1}] has no counterpart in the experimental spectrum. However, in the N_2 matrix, this conformer is present in non-negligible amount. This is quite evident in the 3640−3540 cm^{-1} and 1520−1450 cm^{-1} regions, where the experimental bands at 3615, 1507 and 1456 cm^{-1} are readily ascribed to the IR bands computed for the *trans* conformer at 3641 [ν(OH)], 1500 [δ(CH)$_{as}$] and 1452 cm^{-1} [δ(CH)$_s$], respectively (see also Table 2). Using the integrated absorbance of the bands ascribed to the *trans*/*cis* conformers at 3615/3572 [ν(OH)] and 1507/1492 cm^{-1} [ν(CH)$_{as}$], and corresponding computed IR intensities, the relative amount of the *trans* conformer in the N_2 matrix is estimated to be ~ 15 % (*cis* conformer ~ 85 %), which is significantly higher than that estimated for the vapour phase at room temperature before the deposition and also in the Ar matrix. The reasons behind this discrepancy will be presented in the next sections of this article

4.3. Conformational interconversions of 2CP in an N_2 matrix induced by NIR laser irradiation

The NIR laser irradiations were performed for 2CP isolated in solid N_2, where both conformers could be spectroscopically identified after the matrix deposition. In order to identify adequate vibrational modes to excite matrix-isolated compound, an NIR spectrum was first recorded. Special attention was given to the region in the vicinity of 7000 cm^{-1},

where the first overtones of the OH stretching vibrations [2ν(OH)] are expected to appear. The 7120−6900 cm^{-1} fragment of the recorded NIR spectrum is presented in Figure 4a. The bands centred at ~ 7063 and ~ 6970 cm^{-1} are readily assigned to the 2ν(OH) transitions of the *trans* and *cis* conformers, respectively (Figure 4b). This assignment is supported by the good agreement between the experimental and B3LYP computed 2ν(OH) wavenumbers [*trans* = 7106 cm^{-1} ; *cis* = 6966 cm^{-1}] (Table S3), as well as by the similarity between the profile of the overtone 2ν(OH) and fundamental ν(OH) absorptions (Figures 4a and 4b).

Based on the above information, the sample was irradiated at 7063 and 6970 cm^{-1}, and the effects presented in the difference spectra of mid-IR (Figures 5a and 5c) and NIR (Figure 4c) regions. These difference spectra indicate that when the sample is subjected to NIR laser light at 6970 cm^{-1}, the bands ascribed to the *cis* conformer decrease whereas the bands due to the *trans* conformer increase (Figures 4c and 5a). Enriching the *trans* population in the sample upon NIR irradiation allowed a more comprehensive assignment of the vibrational spectra of this conformer (Table 2). On the other hand, when the laser is tuned at 7063 cm^{-1}, the opposite transformation (*trans* into *cis*) occurs (Figure 5c), thus demonstrating the reversibility of the NIR-induced conformational isomerization (Scheme 1). Similar results were observed upon irradiations at 6987 or 6961 cm^{-1}, which correspond to the centres of the minor components within the 2ν(OH) band profile ascribed to the *cis* conformer (Figure S3).

4.4. Conformational changes of 2CP due to exposure to IR light of the spectrometer globar

In order to examine the possible existence of conformational changes induced by the broadband IR light emitted by the globar of the spectrometer, a new set of experiments was conducted. First, 2CP was deposited in a N_2 matrix at 15 K and, during this process, mid-IR spectra were recorded in the presence of a longpass filter, transmitting IR light only below ~ 1590 cm^{-1} (~19 kJ mol^{-1}). This filter was selected to block any effect regarding the stimulated *cis* → *trans* transformation, which has a computed energy barrier of 25 kJ mol^{-1} (Figure 2). Under these conditions, the *cis* : *trans* population ratio after the deposition was estimated to be 97.5 : 2.5, using the integrated absorbance of the 1507 / 1456 cm^{-1} pair of bands and respective calculated IR intensities. This population ratio is practically coincident with that theoretically predicted for the gas phase at 298.15 K prior to the matrix deposition (see section 4.1). When the filter was removed and the sample let exposed to the unfiltered broadband IR radiation, the bands of the *trans* conformer increased (e.g. at 1507 and 1456

cm^{-1}), while those of the *cis* conformer (e.g. at 1492 cm^{-1}) decreased (Figure 6). This clearly demonstrates that the increment of the population of the *trans* conformer in the N$_2$ matrix relative to the predicted gas-phase population, observed in section 4.2, is caused by the IR radiation emitted by the spectrometer.

The fact that the *trans* conformer was not experimentally detected in the Ar matrix points to the existence of an opposite effect leading to a faster disappearance of this form. Fast conformational decay has been reported previously for other molecules isolated in noble gas matrixes constituted by conformers differing between each other by 180° rotation of an OH group. [26-27, 34-35, 46, 59-60] Moreover, it has been suggested that in an N$_2$ matrix, the formation of specific O−H⋯N$_2$ stabilizing interactions between the host and guest molecules is responsible for the increase of the life-time of the higher-energy conformers as compared to a noble gas matrix.[24, 53, 54] The red-shift of the ν(OH) stretching frequency is frequently used to assess the strength of intermolecular OH interactions.[55] However, because *trans*-2CP was observed in this work only in N$_2$ but not in the Ar matrix, the parent phenol molecule can mimic *trans*-2CP conformer, as in both cases the OH group is not involved in any intramolecular interaction. The red-shift of ν(OH) of parent phenol upon going from Ar (3638 cm^{-1})[56] to N$_2$ (3622 cm^{-1})[57] matrix constitutes 16 cm^{-1}. For comparison, the same red-shift is only 4 cm^{-1} for *cis*-2CP (see Table 2). It is thus expected that the O−H⋯N$_2$ interactions would be stronger for the *trans* conformer, enhancing the relative stability of this form in N$_2$ matrix comparing to the Ar noble gas matrix. This is in accord with calculated binding energies for the 1:1 *trans*-2CP/Ar and *trans*-2CP/N$_2$ OH-bound complexes (see Figure S4).

In order to go deeper into the conformational effects resulting from the spectrometer globar, further experiments were performed. Hence, monochromatic NIR irradiations at 6970 and 7063 cm^{-1} were first undertaken to prepare two different compositions of *cis* and *trans* conformers in the N$_2$ matrix: 75:25 and 92:8, respectively. Then, conformational changes were spectroscopically monitored by letting the sample exposed to the unfiltered broadband IR radiation from the spectrometer globar. It was observed that under these conditions, and independently of the starting conformational composition, a *cis* : *trans* = 85:15 stationary state was achieved after ~ 50 minutes of exposure (Figure 7a). These results show that the unfiltered broadband IR radiation promotes the conformational isomerization of 2CP in both directions (Scheme 1). The variation of the population (y) of any of the two conformers with time (t) nicely fits an exponential function ($y = a + be^{-kt}$), where k is a global rate constant, resulting from the sum of the partial rate constants for the *trans* → *cis* (k_{t-c}) and *cis* → *trans*

($k_{c\text{-}t}$) isomerizations. The following rate constants were estimated from the data fitting: $k =$ 1.4×10^{-3} s^{-1}, $k_{t\text{-}c} = 1.2 \times 10^{-3}$ s^{-1} and $k_{c\text{-}t} = 2.1 \times 10^{-4}$ s^{-1}.

It is conceivable that when the sample is exposed to the spectrometer globar, the excitation of the high-frequency $\nu(OH)$ modes (~ 43 kJ mol^{-1}; much higher in energy than the barrier separating the conformers) would be the main factor responsible for inducing the interconversion between the two conformers. Therefore, in a subsequent experiment, after preparing a sample with an 80:20 conformational *cis* : *trans* ratio, the conformational changes were monitored with the sample only exposed to globar radiation below ~ 2200 cm^{-1} (~26 kJ mol^{-1}; still above the conformational energy barriers). It was observed that under such conditions, the populations of the two conformers also tend to a stationary state but now with a different population ratio (*cis* : *trans* = 90:10), which is achieved after a longer time period (~120 minutes) (Figure 7b). Accordingly, smaller rate constants were obtained by fitting the experimental data to the exponential function given above: $k = 4.3 \times 10^{-4}$ s^{-1} (global constant), $k_{t\text{-}c} = 3.9 \times 10^{-4}$ s^{-1} (*trans* $\rightarrow$ *cis*) and $k_{c\text{-}t} = 4.3 \times 10^{-5}$ s^{-1} (*cis* $\rightarrow$ *trans*). Note that the same stationary state was achieved by starting with a conformational composition slightly shifted towards the most stable form (*cis* : *trans* = 93:7) (Figure 7b).

The kinetic observations reveal that the stationary state of the sample exposed to filtered IR light (blocking above ~ 2200 cm^{-1}) is more shifted towards the most stable conformer, as compared to the stationary state of the sample exposed to unfiltered globar radiation. This observation can be rationalized in terms of the number of excited vibration levels above the energy barrier for the *cis* $\leftrightarrow$ *trans* isomerization in the forward (25 kJ mol^{-1}, 2090 cm^{-1}) or reverse directions (15 kJ mol^{-1}, 1254 cm^{-1}). While in the presence of the 2200 cm^{-1} filter only the excitation of the $\nu(CN)$ vibration assigned to the *cis* form (~ 2230 cm^{-1}, near the limit of the filter cuttof) can promote the *cis* $\rightarrow$ *trans* conversion, a higher number of absorptions due to the *trans* form, found between 1254 and 2200 cm^{-1} (Table 2), can promote the *trans* $\rightarrow$ *cis* transformation. However, as it will be shown below, this interpretation is far from being complete, since besides the over the barrier conformational isomerization, hydrogen tunneling also contributes to the *trans* $\rightarrow$ *cis* isomerization process.

4.5. Tunneling in the *trans* $\rightarrow$ *cis* isomerization

2CP in an N$_2$ matrix at 15 K with an initial *cis* : *trans* conformational composition of 85:15, was kept in the dark for several hours and the spectroscopic monitoring was made

under the presence of a filter blocking the IR radiation above ~ 1170 cm^{-1} (~14 kJ mol^{-1}). As the cutoff of this filter is below the computed energy barrier for the conformational isomerization in any of the two directions (Figure 2), no photoinduced isomerization is expected to take place. The IR spectrum recorded after letting the sample 13 hours in the dark clearly shows that the *trans* conformer isomerizes to the *cis* conformer (Figure 8). The progress of this spontaneous transformation was followed by collecting a few IR spectra while keeping the sample completely blocked from any IR light in the intervals between collections. The population variation of the *trans* conformer was measured by integration of the absorption band at ~1096 cm^{-1} (Figure 9 ; closed red circles).[58] A similar *trans* → *cis* kinetic decay was observed when the sample was continuously exposed to the globar IR radiation below ~ 1170 cm^{-1} (Figure 9; open red circles). This confirms that such range of IR radiation does not induce changes in the conformational distribution of 2CP. Fitting the kinetic data to a single-exponential equation (y = e^{-kt}), a rate constant $k = 3.6 \times 10^{-4}$ s^{-1} was estimated for the spontaneous *trans* → *cis* decay, corresponding to a half-life time $t_{1/2} = 32$ min. At a temperature as low as 15 K there is simply not enough thermal energy to induce the isomerization reaction over a postulated barrier of ~15 kJ mol^{-1}. Therefore, the observed conformational isomerization must occur through quantum tunneling of the hydrogen atom (Scheme 1). To unequivocally confirm this hypothesis, kinetic measurements were also carried out at 10 K (Figure 9; squares) and 20 K (Figure 9; triangles). The rate constants obtained from the exponential fits are $k = 2.8 \times 10^{-4}$ s^{-1} ($t_{1/2} = 40$ min) at 10 K and $k = 3.5 \times 10^{-4}$ s^{-1} ($t_{1/2} = 33$ min) at 20 K. Thus, as the variation of the absolute temperature by a factor of two has a negligible effect on the estimated rate constants, the disappearance of the *trans* conformer in an N$_2$ matrix, both in dark conditions or exposed to IR radiation below ~ 1170 cm^{-1}, can only be due to a pure quantum tunneling reaction. Hydrogen tunneling was also found to play an important role in the isomerization between the *cis* and *trans* conformers of two other phenol derivatives: hydroquinone[39] and tetrachlorohydroquinone,[59] for which the torsional barriers in the direction of the conformational relaxation, 11 and 19 kJ mol^{-1}, respectively, are of the same order of the value computed by us for 2CP (15 kJ mol^{-1}).

It is now interesting to analyse the contribution of tunneling in the presence of filtered (below ~ 2200 cm^{-1}) and unfiltered IR radiation from the globar. The rate constant measured under conditions of exposure of the sample to globar radiation below ~ 2200 cm^{-1} ($k_{t-c} = 3.9 \times 10^{-4}$ s^{-1}) is on the same order of magnitude of the measured tunneling rate constant at 15 K (3.6 × 10^{-4} s^{-1}). This indicates that tunneling is the dominant cause of the *trans* → *cis*

isomerization in the presence of IR light below ~ 2200 cm^{-1}. When the sample is exposed to unfiltered IR globar light, the excitation of the OH stretching vibrations (including both the fundamental and overtone transitions) and possibly of other modes, lead to a considerable increase of the *trans* $\rightarrow$ *cis* rate constant ($k_{t\text{-}c} = 1.2 \times 10^{-3}$ s^{-1}). Nevertheless, the tunneling contribution is still significant, representing ~ 30 % of the overall *trans* $\rightarrow$ *cis* rate constant. We demonstrated therefore that 2CP is a very interesting case where IR-radiation and hydrogen atom tunneling affect the conversion processes between two conformers on the same time scale.

5. CONCLUSION

Conformational isomerism in 2CP was studied for the matrix-isolated compound, using infrared spectroscopy supported by quantum chemical calculations. This molecule has two planar conformers: *cis* and *trans*, the first being more stable due to the formation of a weak O−H···N≡C hydrogen bond-like interaction.

Narrowband irradiation of 2CP isolated in solid N$_2$ with NIR laser light tuned at the wavenumbers of the 2ν(OH) transitions of the conformers (6970 cm^{-1} for *cis* and 7063 cm^{-1} for *trans*) led to a bidirectional conversion between the two forms. To the best of our knowledge, observation of this type of processes in phenol type compounds had only been reported for gallic acid.[31] This also allowed, for the first time, the spectroscopic characterization of the high-energy *trans* conformer.

The effect of the spectrometer broadband IR source was investigated by preparing different relative populations of the two 2CP conformers in N$_2$ matrix and subjected it to diverse experimental conditions (kept in the dark or exposed to the spectrometer globar using different cutoff filters). The rate constants for the isomerization processes (*trans* $\rightarrow$ *cis* and *cis* $\rightarrow$ *trans*) were measured under different conditions of exposure to IR light of the spectrometer and compared with the *trans* $\rightarrow$ *cis* tunneling rate constant. Such comparison highlighted the relevance of hydrogen tunneling, even when the sample was exposed to the unfiltered IR light. Under these conditions, a *cis* : *trans* = 85:15 stationary state was observed and tunneling was determined to account for about 30 % of the overall *trans* $\rightarrow$ *cis* rate constant. The performed detailed analyses of the IR-radiation and tunneling effects on the conformational isomerization reactions, together with the expected stabilization of the more polar *trans* conformer in the N$_2$ matrix through a specific interaction between the OH group

and the N_2 molecules, also allowed to explain the different *cis*:*trans* population-ratios observed after isolating monomers of 2CP in Ar and N_2 matrixes.

Overall, it was concluded that 2CP represents a rare and interesting case where the broadband IR-radiation and tunneling effects are entangled, affecting the conformational interconversion on the time scale of the same order (tens of minutes).

SUPPORTING INFORMATION

The Supporting Information is available free of charge on the ACS Publications website at DOI: xxxxxxxxxxxxxxx

Table S1, with Cartesian coordinates for the *cis* and *trans* conformers of 2CP optimized at different levels of theory; Table S2, with definition of internal coordinates used in the normal mode analysis of 2CP; Table S3, with the overtone transitions calculated for the *cis* and *trans* conformers of 2CP obtained through anharmonic vibrational calculations carried out at the B3LYP/6-31++G(d,p) level of theory; Tables S4 and S5, with the B3LYP/6-311++G(d,p) calculated harmonic wavenumbers, absolute IR intensities and potential energy distributions (PED) for the *cis* and *trans* conformers of 2CP; Figure S1, showing a single beam spectrum recorded with a ETC EverGlo IR source and transmittance spectra of the longpass filters used in the present work; Figure S2, representing the atom numbering used in 2CP for the definition of the internal coordinates; Figure S3, illustrating the spectral changes observed after irradiating monomers of 2CP isolated in an N_2 matrix (15 K) with NIR laser light tuned at 6987 cm^{-1}; Figure S4 with the MP2/6-311++G(3df,3pd) optimized geometries of 1:1 OH-bound complexes of *trans*-2CP with N_2 and Ar, including the BSSE corrected binding energies; Figure S5, showing a fragment of IR spectra recorded during the permanence of an N_2 matrix in the dark, after being enriched with the *trans* form by performing NIR irradiations at 6970 cm^{-1}.

REFERENCES

(1) Abraham, M. H.; Abraham, R. J.; Aliev, A. E.; Tormena, C. F. Is There an Intramolecular Hydrogen Bond in 2-halophenols? A Theoretical and Spectroscopic Investigation. *Phys. Chem. Chem. Phys.* **2015,** *17*, 25151-25159.

(2) Imhof, P.; Kleinermanns, K. Dispersed Fluorescence Spectra and Ab Initio Calculations of o-Cyanophenol. *J. Phys. Chem. A* **2001,** *105*, 8922-8925.

(3) Conrad, A. R.; Barefoot, N. Z.; Tubergen, M. J. Rotational Spectra of o-, m-, and p-Cyanophenol and Internal Rotation of p-Cyanophenol. *Phys. Chem. Chem. Phys.* **2010,** *12*, 8350-8356.

(4) Beswick, C.; Kubicki, M.; Codding, P. W. o-Cyanophenol. *Acta Crystallogr., Sect. C: Cryst. Struct. Commun.* **1996,** *52*, 3171-3173.

(5) Matos, M. A. R.; Miranda, M. S.; Morais, V. M. F. Thermochemical Study of the Cyanophenol Isomers. *Struct. Chem.* **2004,** *15*, 103-116.

(6) Carlson, G. L.; Fateley, W. G. Torsional Frequencies and Conformational Equilibriums of o-Substituted Phenols. *J. Phys. Chem.* **1973,** *77*, 1157-1163.

(7) Zhang, L.; Peslherbe, G. H.; Muchall, H. M. Ultraviolet Absorption Spectra of Substituted Phenols: A Computational Study. *Photochem. Photobiol.* **2006,** *82*, 324-331.

(8) Lee, K.-K.; Park, K.-H.; Choi, J.-H.; Ha, J.-H.; Jeon, S.-J.; Cho, M. Ultrafast Vibrational Spectroscopy of Cyanophenols. *J. Phys. Chem. A* **2010,** *114*, 2757-2767.

(9) Broquier, M.; Lahmani, F.; Zehnacker-Rentien, A.; Brenner, V.; Millié, P.; Peremans, A. Hydrogen-Bonded Bridges in Complexes of o-Cyanophenol: Laser-Induced Fluorescence and IR/UV Double-Resonance Studies. *J. Phys. Chem. A* **2001,** *105*, 6841-6850.

(10) Binev, Y. I.; Georgieva, M. K.; Daskalova, L. I. Spectrochemical, Ab Initio and Density Functional Studies on the Conversion of 2-Hydroxybenzonitrile (o-Cyanophenol) Into the Oxyanion. *Spectrochim. Acta, Part A* **2004,** *60*, 2601-2610.

(11) Nunes, C. M.; Pinto, S. M. V.; Reva, I.; Fausto, R. On the Photochemistry of 1,2-Benzisoxazole: Capture of Elusive Spiro-2H-azirine and Ketenimine Intermediates. *Eur. J. Org. Chem.* **2016**, 4152-4158.

(12) Barnes, A. J. Matrix Isolation Vibrational Spectroscopy as a Tool for Studying Conformational Isomerism. *J. Mol. Struct.* **1984,** *113*, 161-174.

(13) Fausto, R.; Khriachtchev, L.; Hamm, P. Conformational Changes in Cryogenic Matrices. In *Physics and Chemistry at Low Temperatures*, Khriachtchev, L., Ed. Pan Stanford Publishing: Singapore, 2010; pp 51-84.

(14) Baldeschwieler, J. D.; Pimentel, G. C. Light-Induced Cis-Trans Isomerization of Nitrous Acid Formed by Photolysis of Hydrazoic Acid and Oxygen in Solid Nitrogen. *J. Chem. Phys.* **1960,** *33*, 1008-1015.

(15) Hall, R. T.; Pimentel, G. C. Isomerization of Nitrous Acid: An Infrared Photochemical Reaction. *J. Chem. Phys.* **1963,** *38*, 1889-1897.

(16) Pettersson, M.; Lundell, J.; Khriachtchev, L.; Räsänen, M. IR Spectrum of the Other Rotamer of Formic Acid, cis-HCOOH. *J. Am. Chem. Soc.* **1997,** *119*, 11715-11716.

(17) Sharma, A.; Reva, I.; Fausto, R. Conformational Switching Induced by Near-Infrared Laser Irradiation. *J. Am. Chem. Soc.* **2009,** *131*, 8752-8753.

(18) Lopes Jesus, A. J.; Reva, I.; Araujo-Andrade, C.; Fausto, R. Conformational Switching by Vibrational Excitation of a Remote NH Bond. *J. Am. Chem. Soc.* **2015,** *137*, 14240-11243

(19) Maçôas, E. M. S.; Khriachtchev, L.; Pettersson, M.; Fausto, R.; Räsänen, M. Rotational Isomerism in Acetic Acid: The First Experimental Observation of the High-Energy Conformer. *J. Am. Chem. Soc.* **2003,** *125*, 16188-16189.

(20) Halasa, A.; Lapinski, L.; Reva, I.; Rostkowska, H.; Fausto, R.; Nowak, M. J. Near-Infrared Laser-Induced Generation of Three Rare Conformers of Glycolic Acid. *J. Phys. Chem. A* **2014,** *118*, 5626-5635.

(21) Halasa, A.; Lapinski, L.; Reva, I.; Rostkowska, H.; Fausto, R.; Nowak, M. J. Three Conformers of 2-Furoic Acid: Structure Changes Induced with Near-IR Laser Light. *J. Phys. Chem. A* **2015,** *119*, 1037-1047.

(22) Maçôas, E. M. S.; Khriachtchev, L.; Pettersson, M.; Lundell, J.; Fausto, R.; Räsänen, M. Infrared-Induced Conformational Interconversion in Carboxylic Acids Isolated in Low-Temperature Rare-Gas Matrices. *Vib. Spectrosc.* **2004,** *34*, 73-82.

(23) Halasa, A.; Lapinski, L.; Rostkowska, H.; Reva, I.; Nowak, M. J. Tunable Diode Lasers as a Tool for Conformational Control: The Case of Matrix-Isolated Oxamic Acid. *J. Phys. Chem. A* **2015,** *119*, 2203-2210.

(24) Reva, I.; Nunes, C. M.; Biczysko, M.; Fausto, R. Conformational Switching in Pyruvic Acid Isolated in Ar and N2 Matrixes: Spectroscopic Analysis, Anharmonic Simulation, and Tunneling. *J. Phys. Chem. A* **2015,** *119*, 2614-2627.

(25) Nunes, C. M.; Lapinski, L.; Fausto, R.; Reva, I. Near-IR laser Generation of a High-Energy Conformer of L-Alanine and the Mechanism of its Decay in a Low-Temperature Nitrogen Matrix. *J. Chem. Phys.* **2013,** *138*, 125101.

(26) Bazsó, G.; Magyarfalvi, G.; Tarczay, G. Tunneling Lifetime of the ttc/VIp Conformer of Glycine in Low-Temperature Matrices. *J. Phys. Chem. A* **2012,** *116*, 10539-10547.

(27) Bazsó, G.; Najbauer, E. E.; Magyarfalvi, G.; Tarczay, G. Near-Infrared Laser Induced Conformational Change of Alanine in Low-Temperature Matrixes and the Tunneling Lifetime of its Conformer VI. *J. Phys. Chem. A* **2013,** *117*, 1952-1962.

(28) Lapinski, L.; Reva, I.; Rostkowska, H.; Fausto, R.; Nowak, M. J. Near-IR-Induced, UV-Induced, and Spontaneous Isomerizations in 5-Methylcytosine and 5-Fluorocytosine. *J. Phys. Chem. B* **2014,** *118*, 2831-2841.

(29) Lapinski, L.; Nowak, M. J.; Reva, I.; Rostkowska, H.; Fausto, R. NIR-Laser-Induced Selective Rotamerization of Hydroxy Conformers of Cytosine. *Phys. Chem. Chem. Phys.* **2010,** *12*, 9615-9618.

(30) Reva, I.; Nowak, M. J.; Lapinski, L.; Fausto, R. Spontaneous Tunneling and Near-Infrared-Induced Interconversion Between the Amino-Hydroxy Conformers of Cytosine. *J. Chem. Phys.* **2012,** *136*, 064511.

(31) Justino, L. L. G.; Reva, I.; Fausto, R. Thermally and Vibrationally Induced Conformational Isomerizations, Infrared Spectra, and Photochemistry of Gallic Acid in Low-Temperature Matrices. *J. Chem. Phys.* **2016,** *145*, 014304.

(32) Takeuchi, H.; Tasumi, M. Infrared-Induced Conformational Isomerization of Ethylene Glycol in a Low-Temperature Argon Matrix. *Chem. Phys.* **1983,** *77*, 21-34.

(33) Lopes Jesus, A. J.; Reva, I.; Araujo-Andrade, C.; Fausto, R. Conformational Changes in Matrix-Isolated 6-Methoxyindole: Effects of the Thermal and Infrared Light Excitations. *J. Chem. Phys.* **2016,** *144*, 124306.

(34) Ryazantsev, S. V.; Feldman, V. I.; Khriachtchev, L. Conformational Switching of HOCO Radical: Selective Vibrational Excitation and Hydrogen-Atom Tunneling. *J. Am. Chem. Soc.* **2017,** *139*, 9551-9557.

(35) Pettersson, M.; Maçôas, E. M. S.; Khriachtchev, L.; Lundell, J.; Fausto, R.; Räsänen, M. Cis→Trans Conversion of Formic Acid by Dissipative Tunneling in Solid Rare Gases: Influence of Environment on the Tunneling Rate. *J. Chem. Phys.* **2002,** *117*, 9095-9098.

(36) Wagner, J. P.; Reisenauer, H. P.; Hirvonen, V.; Wu, C.-H.; Tyberg, J. L.; Allen, W. D.; Schreiner, P. R. Tunnelling in Carbonic Acid. *Chem. Commun.* **2016,** *52*, 7858-7861.

(37) Amiri, S.; Reisenauer, H. P.; Schreiner, P. R. Electronic Effects on Atom Tunneling: Conformational Isomerization of Monomeric Para-Substituted Benzoic Acid Derivatives. *J. Am. Chem. Soc.* **2010,** *132*, 15902-15904.

(38) Gerbig, D.; Schreiner, P. R. Hydrogen-Tunneling in Biologically Relevant Small Molecules: The Rotamerizations of α-Ketocarboxylic Acids. *J. Phys. Chem. B* **2015,** *119*, 693-703.

(39) Akai, N.; Kudoh, S.; Takayanagi, M.; Nakata, M. Cis–Trans Isomerization Equilibrium in Hydroquinone in Low-Temperature Argon and Xenon Matrices Studied by FTIR Spectroscopy. *Chem. Phys. Lett.* **2002,** *356*, 133-139.

(40) Frisch, M. J.; Trucks, G. W.; Schlegel, H. B.; Scuseria, G. E.; Robb, M. A.; Cheeseman, J. R.; Scalmani, G.; Barone, V.; Mennucci, B.; Petersson, G. A., et al. *GAUSSIAN 09, Revision D.01*, Gaussian, Inc.: Wallingford CT, 2013.

(41) Becke, A. D. Density-Functional Exchange-Energy Approximation with Correct Asymptotic-Behavior. *Phys. Rev. A* **1988,** *38*, 3098-3100.

(42) Lee, C. T.; Yang, W. T.; Parr, R. G. Development of the Colle-Salvetti Correlation-Energy Formula into a Functional of the Electron-Density. *Phys. Rev. B* **1988,** *37*, 785-789.

(43) Vosko, S. H.; Wilk, L.; Nusair, M. Accurate Spin-Dependent Electron Liquid Correlation Energies for Local Spin Density Calculations: a Critical Analysis. *Can. J. Phys.* **1980,** *58*, 1200-1211.

(44) Møller, C.; Plesset, M. S. Note on an Approximation Treatment for Many-Electron Systems. *Phys. Rev.* **1934,** *46*, 618-622.

(45) Pople, J. A.; Head-Gordon, M.; Raghavachari, K. Quadratic Configuration Interaction. A General Technique for Determining Electron Correlation Energies. *J. Chem. Phys.* **1987,** *87*, 5968-5975.

(46) Zhurko, G. A. C., Version 1.8. http://www.chemcraftprog.com, 2016 (last accessed on January, 2019).

(47) Barone, V. Anharmonic Vibrational Properties by a Fully Automated Second-Order Perturbative Approach. *J. Chem. Phys.* **2005,** *122*, 014108.

(48) Bloino, J.; Barone, V. A Second-Order Perturbation Theory Route to Vibrational Averages and Transition Properties of Molecules: General Formulation and Application to Infrared and Vibrational Circular Dichroism Spectroscopies. *J. Chem. Phys.* **2012,** *136*, 124108.

(49) Glendening, E. D.; Reed, A. E.; Carpenter, J. E.; Weinhold, F. *NBO Version 3.1.*

(50) Korth, H.-G.; de Heer, M. I.; Mulder, P. A DFT Study on Intramolecular Hydrogen Bonding in 2-Substituted Phenols: Conformations, Enthalpies, and Correlation with Solute Parameters. *J. Phys. Chem. A* **2002,** *106*, 8779-8789.

(51) Lopes Jesus, A. J.; Rosado, M. T. S.; Reva, I.; Fausto, R.; Eusébio, M. E.; Redinha, J. S. Conformational Study of Monomeric 2,3-Butanediols by Matrix-Isolation Infrared Spectroscopy and DFT Calculations. *J. Phys. Chem. A* **2006,** *110*, 4169-4179.

(52) Reva, I.; Lopes Jesus, A. J.; Rosado, M. T. S.; Fausto, R.; Ermelinda Eusébio, M.; Redinha, J. S. Stepwise Conformational Cooling Towards a Single Isomeric State in the Four Internal Rotors System 1,2-Butanediol. *Phys. Chem. Chem. Phys.* **2006,** *8*, 5339-5349.

(53) Lopes, S.; Domanskaya, A. V.; Fausto, R.; Räsänen, M.; Khriachtchev, L. Formic and Acetic Acids in a Nitrogen Matrix: Enhanced Stability of the Higher-Energy Conformer. *J. Chem. Phys.* **2010,** *133*, 144507.

(54) Marushkevich, K.; Räsänen, M.; Khriachtchev, L. Interaction of Formic Acid with Nitrogen: Stabilization of the Higher-Energy Conformer. *J. Phys. Chem. A* **2010,** *114*, 10584-10589.

(55) Rozenberg, M.; Shoham, G.; Reva, I.; Fausto, R. A Correlation between the Proton Stretching Vibration Red Shift and the Hydrogen Bond Length in Polycrystalline Amino Acids and Peptides. *Phys. Chem. Chem. Phys.* **2005,** *7*, 2376-2383.

(56) Giuliano, B. M.; Reva, I.; Lapinski, L.; Fausto, R. Infrared Spectra and Ultraviolet-Tunable Laser Induced Photochemistry of Matrix-Isolated Phenol and Phenol-d5. *J. Chem. Phys.* **2012,** *136*, 024505.

(57) Cao, Q.; Andrijchenko, N.; Ahola, A.-E.; Domanskaya, A.; Räsänen, M.; Ermilov, A.; Nemukhin, A.; Khriachtchev, L. Interaction of Phenol with Xenon and Nitrogen: Spectroscopic and Computational Characterization. *J. Chem. Phys.* **2012,** *137*, 134305.

(58) The band at ~ 1096 cm^{-1} contains two components: one centered at 1097 cm^{-1} (assigned to cis) and another one centered at 1095 cm^{-1} (assigned to trans), Figure S5. Since the component assigned to the *trans* conformer has an intrinsic IR intensity 36 times higher than that of the *cis* conformer (54.0 km mol^{-1} vs. 1.5 km mol^{-1}, see Table 2), it has been assumed that the variation of the intensity of this band during the spontaneous transformation is essentially atributed to the *trans* conformer. Moreover, to remove the contribution of the cis conformer, the intensity of this band in a spectrum recorded after keeping the sample several hours in dark (which would correspond to 100 % cis) was subtracted from the intensities of the same absorption in the spectra recorded during the kinetics measurements.

(59) Akai, N.; Kudoh, S.; Nakata, M. Photoisomerization and Tunneling Isomerization of Tetrachlorohydroquinone in a Low-Temperature Argon Matrix. *J. Phys. Chem. A* **2003,** *107*, 3655-3659.
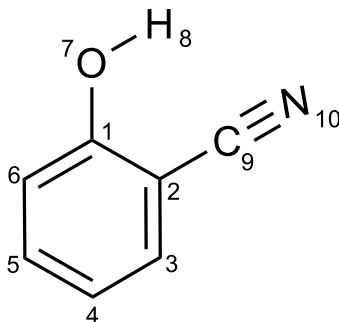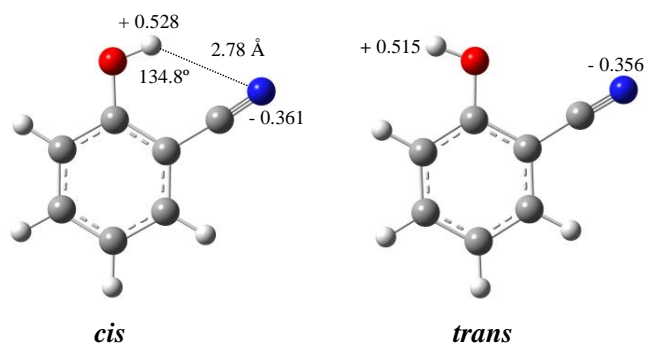
Chart 1. Molecular structure of 2-cyanophenol (2CP) and numbering of selected atoms.
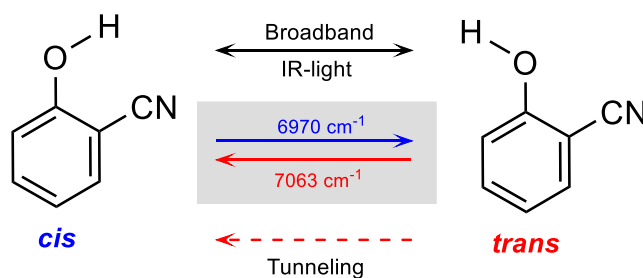
Scheme 1. IR-induced and tunneling isomerization on the conformers of 2CP isolated in an N_2 matrix at 15 K.

+ 0.528
2.78 Å
134.8°
- 0.361
cis

+ 0.515
- 0.356
trans

Figure 1. Geometries of the *cis* and *trans* conformers of 2CP optimized at the QCISD/6-31++G(d,p) level of theory, including some parameters related with the intramolecular hydrogen-bond-like interaction: H···N distance (Å) and O–H···N angle (degrees), and the natural charges at the hydrogen and nitrogen atoms calculated from an NBO analysis at the QCISD level.
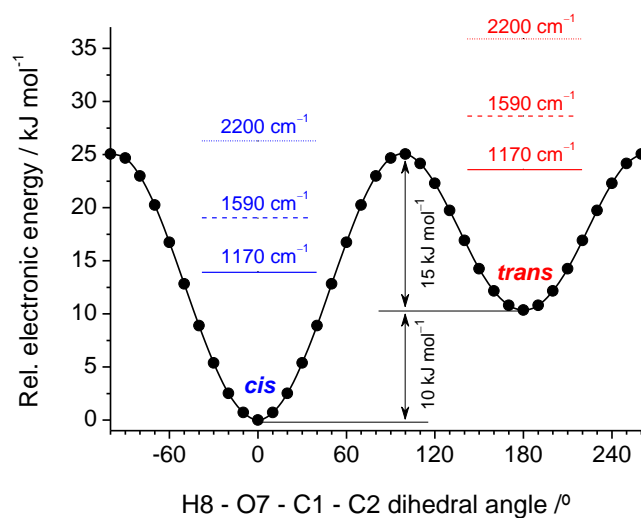
Figure 2. Relaxed potential energy scan calculated at the B3LYP/6-311++G(d,p) level of theory as a function of the internal rotation of the O–H group in 2CP. Horizontal blue or and red lines indicate the cutoff energies of the longpass filters relative to *cis* (left, blue) and *trans* (right, red) conformers, respectively: ~2200 cm^{-1} (dotted lines); ~1590 cm^{-1} (dashed lines); ~1170 cm^{-1} (solid lines).
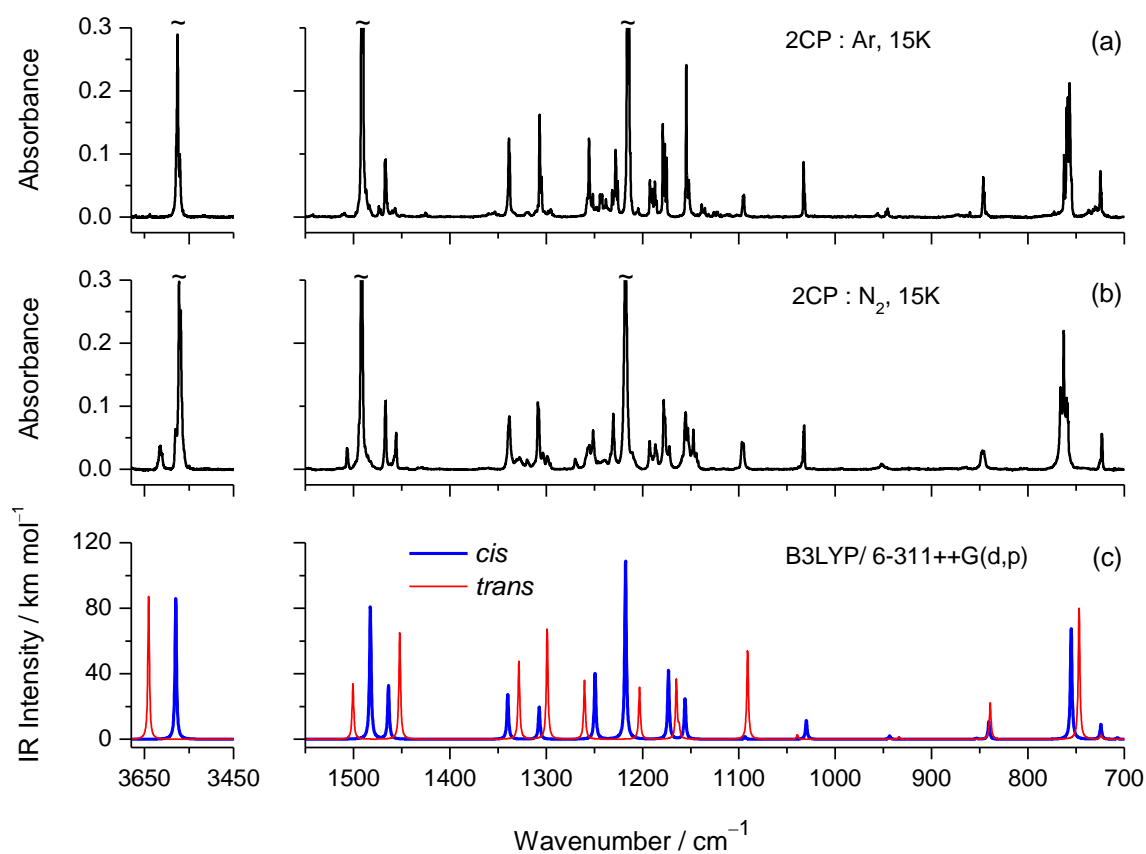
Figure 3. Experimental mid-IR spectra of 2CP isolated in **(a)** Ar, and **(b)** N_2 matrixes at 15 K, compared with **(c)** IR spectra of two 2CP conformers (*cis*: bold blue trace; *trans*: thin red trace) computed at the B3LYP/6-311++G(d,p) level of theory. Details of the spectra simulation are given in the computational section.
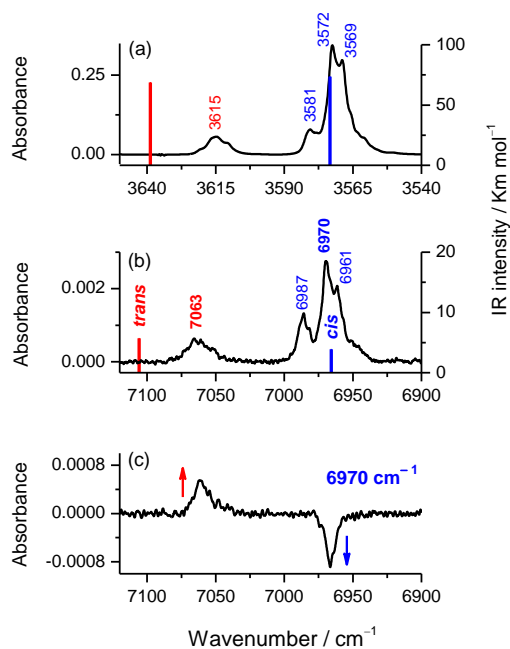
Figure 4. Fragments of the **(a)** mid-IR and **(b)** NIR spectra of 2CP isolated in an N_2 matrix at 15 K, showing the absorptions assigned to the $\nu(OH)$ and $2\nu(OH)$ vibrations of the *cis* (blue) and *trans* (red) conformers. **(c)** Spectral changes in the NIR region induced upon irradiation at 6970 cm^{-1}. Sticks in frame (a) correspond to the B3LYP harmonic wavenumbers (scaled) and IR intensities calculated for the $\nu(OH)$ modes, while sticks in frame (b) correspond to B3LYP anharmonic wavenumbers (unscaled) and IR intensities calculated for the $2\nu(OH)$ overtones.
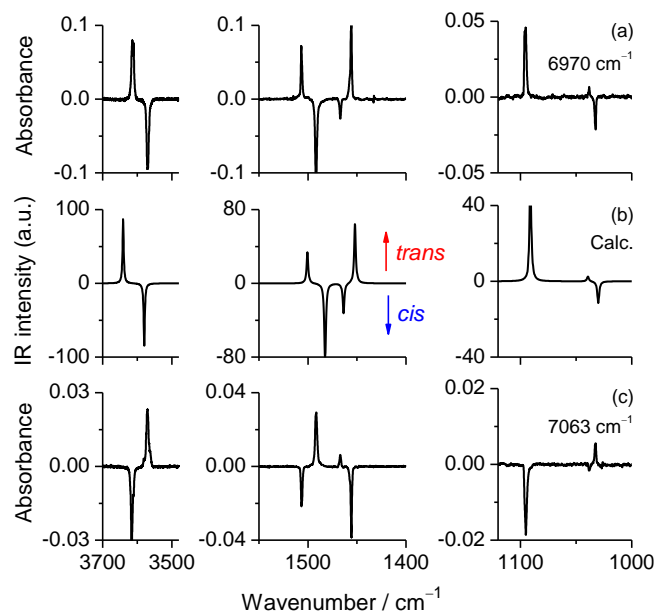
Figure 5. Selected mid-IR regions showing changes in the IR spectra of monomeric 2CP (N_2, 15 K) induced by laser irradiations at wavenumbers assigned to the $2\nu(OH)$ transitions of the *cis* (6970 cm^{-1}) and *trans* (7063 cm^{-1}) forms: **(a)** Changes induced after 30 min of irradiation at 6970 cm^{-1}; **(c)** Changes induced after 10 min of irradiation at 7063 cm^{-1}. Positive bands grow up during the irradiations. **(b)** Calculated difference spectrum showing quantitative transformation of the *cis* into *trans* form (*trans* "minus" *cis*), simulated from the results of the B3LYP harmonic vibrational calculations.
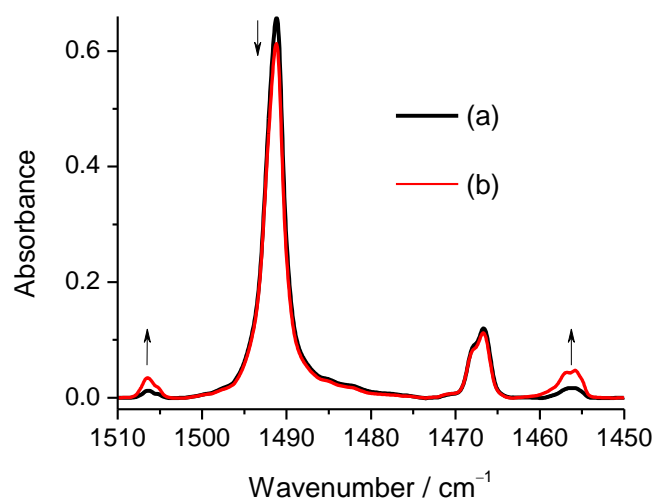
Figure 6. Fragment of the mid-IR spectrum of 2CP isolated in a N_2 matrix at 15 K: **(a)** recorded immediately after the matrix deposition in the presence of a longpass filter transmitting only IR radiation below ~ 1590 cm^{-1}; **(b)** recorded after removing the filter and let the sample exposed during 30 min to the spectrometer globar.
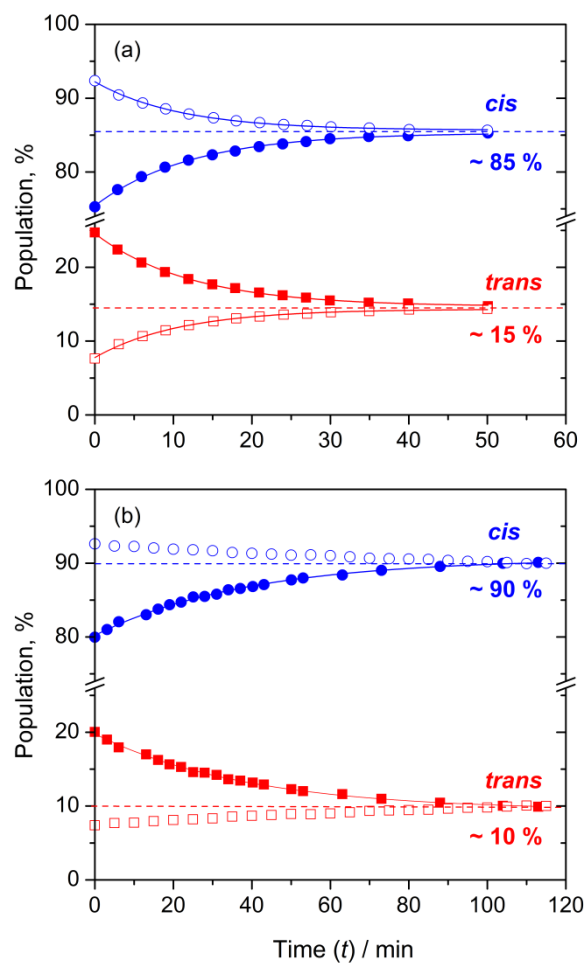
Figure 7. Time evolution of the population of the *cis* (circles) and *trans* (squares) conformers of 2CP in an N_2 matrix during the exposure to **(a)** unfiltered and **(b)** filtered (below ~ 2200 cm^{-1}) broadband IR-light emitted by the spectrometer source. In both cases the initial conformational compositions were obtained by irradiating the sample at 6970 cm^{-1} (closed symbols) or 7063 cm^{-1} (open symbols). Solid curves are the best possible fits of the experimental data to a $y = a + be^{-kt}$ exponential function (for all fits $R^2 = 0.998$).
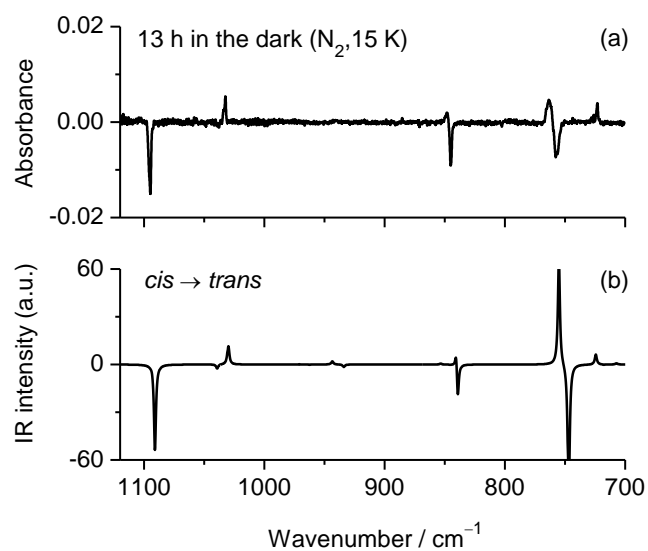
Figure 8. **(a)** Experimental difference spectrum showing intensity changes resulting from keeping an enriched sample with the *trans* conformer (N₂, 15 K) in the dark for 13 hours (negative bands correspond to those decreasing during the dark kinetics). The IR-spectrum was collected using a longpass filter transmitting below ~ 1170 cm⁻¹. **(b)** B3LYP computed difference spectrum for the quantitative *trans* → *cis* transformation.
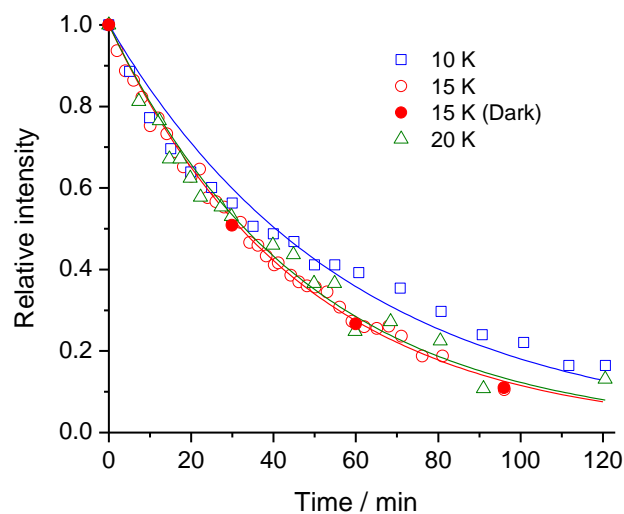
Figure 9. Decay kinetics of the *trans* conformer of 2CP in an N_2 matrix at 10 K (squares), 15 K (open circles) and 20 K (triangles) in the presence of a filter transmitting only IR radiation below ~ 1170 cm^{-1}, and at 15 K in dark conditions (closed circles). The decay process was followed by integration of the band at 1096 cm^{-1}. Solid curves represent the best possible single exponential fits to the experimental points ($R^2 = 0.97 - 0.99$).

Table 1. Electronic energy (ΔE_{el}), zero-point corrected energy (ΔE_0) and Gibbs energy at 298.15 K (ΔG), calculated for the *trans* conformer of 2CP relative to the most stable *cis* form at three different levels of theory, and equilibrium population of the *trans* conformer at 298.15 K.

Level of theory	ΔE_{el} [a]	ΔE_0 [a,b]	ΔG (298.15K) [a]	Population (298.15 K, %) [c]
B3LYP/6-311++G(d,p)	10.25	9.62	9.42	2.2
MP2/6-311++G(3df,3pd)	9.89	9.45	9.30	2.5
QCISD/6-31++G(d,p)	8.32	–	–	–

[a] Relative energies (*trans* − *cis*) in kJ mol^{-1}.
[b] $E_0 = E_{el} + ZPVE$ (zero-point vibrational energy).
[c] Estimated from a Boltzmann distribution based on the ΔG value. The sum of *cis* and *trans* populations totalizes 100 %.

Table 2. Bands observed in the IR spectrum of 2CP isolated in nitrogen (N$_2$) and argon (Ar) matrixes, compared with the harmonic wavenumbers ($\tilde{\nu}$ / cm^{-1}) and absolute intensities (I / km mol^{-1}) calculated for the *cis* and *trans* conformers at the B3LYP/6-311++G(d,p) level of theory.

Experimental[a]		Calc. *cis*		Calc. *trans*		Approximate description[c]
N$_2$, 15 K	Ar, 15 K	$\tilde{\nu}$[b]	I	$\tilde{\nu}$[b]	I	
3615 (vw)	–	–	–	3641	87.2	ν(OH)
3572 (s, split)	3576 (s, split)	3580	86.0	–	–	ν(OH)
2239 (vw)	–	–	–	2287	39.3	ν(CN)
2230 (w)	2228 (vw)	2269	64.7	–	–	ν(CN)
1618 (w)	1621 (w, split)	1620	43.3	–	–	ν_3(CC)$_s$
1613 (vw sh)	–	–	–	1612	43.3	ν_3(CC)$_s$
1590 (m)	–	–	–	1591	24.6	ν_1(CC)$_s$; ν_2(CC)$_s$
1579 (w)	1581 (w)	1580	38.8	–	–	ν_1(CC)$_s$; ν_2(CC)$_s$
1507 (vw)	–	–	–	1500	33.9	δ_1(CH)$_{as}$
1492 (vs)	1491 (vs, split)	1482	81.0	–	–	δ_1(CH)$_{as}$
–	1474 /1472 (vw)	–	–	–	–	–
1467 (w)	1467 (w)	1464	32.8	–	–	δ_2(CH)$_s$
1456 (vw)	–	–	–	1452	65.1	δ_2(CH)$_s$
1338 (vw)	1339 (w)	1340	27.5	–	–	δ(COH)
1327 (vw)	–	–	–	1328	47.6	ν_3(CC)$_{as}$; δ(COH)
1308 (w)	1307/1304 (w)	1307	19.8	–	–	ν(CO) ; ν_2(CC)$_{as}$
1303/1299 (vw)	–	–	–	1299	67.3	δ_1(CH)$_s$
1269 (vw)	–	–	–	1260	36.2	ν(CO)
1255/1251 (vw)	1255/1252 (w)	1249	40.5	–	–	ν(CO) ; ν_2(CC)$_s$; δ_1(CH)$_s$
–	1244/1242 (vw)	–	–	–	–	–
1230 (vw)	1228 (w, split)	–	–	–	–	–
–	1238 (vw)	–	–	–	–	–
1218 (vs)	1214 (vs, split)	1218	109.1	–	–	δ(COH) ; ν(CC)$_{CN}$
1211 (vw, sh)	–	–	–	1203	31.9	ν(CC)$_{CN}$; δ(COH)
1193-1185 (vw)	1193-1185 (vw)	–	–	–	–	–
1178/1172 (w)	1179 (w, split)	1173	42.1	–	–	δ_2(CH)$_{as}$; δ_1(CH)$_s$
1160 (vw, sh)	–	–	–	1165	36.2	δ(COH) ; δ_1(CH)$_s$; δ_2(CH)$_{as}$
1155/1153 (vw)	1155/1152 (m)	1156	24.7	–	–	δ_2(CH)$_{as}$
1147 (vw)	–	–	–	–	–	–
–	1139/1135 (vw)	–	–	–	–	–
1096 (vw)	1095 (vw)	1093	1.5	1091	54.0	ν_3(CC)$_{as}$; δ(ring)
1038 (vw)	–	–	–	1039	2.7	ν_1(CC)$_{as}$; δ_1(CH)$_{as}$; ν_1(CC)$_s$
1032 (vw)	1033 (vw)	1030	11.5	–	–	ν_1(CC)$_{as}$
952 (vw)	956/945 (vw)	944	2.1	–	–	γ(CH)$_{as}$
846 (vw)	846 (vw)	841	10.9	839	22.2	δ(ring)
763 (m, split)	757 (m, split)	755	67.9	747	80.0	γ(CH)$_s$
723 (vw)	725 (vw)	724	9.0	724	2.7	δ(ring)$_{as'}$
565 (vw)	565/564 (vw)	570	2.6	–	–	τ(ring)
558 (vw)	557 (vw)	557	5.2	–	–	δ(ring)$_{as'}$
496 (w)	493 (vw, split)	494	10.7	496	11.4	γ(CO) + γ(CC)$_{CN}$
–	–	412	109.2	320	112.1	τ(COH)

[a] Experimental intensities are given in qualitative terms: vs = very strong; s = strong; m = medium; w = weak; vw = very weak; sh = shoulder. Because of their minor relevance for the present study, absorptions bands falling in the 3300 – 2800 cm^{-1} region, which are assigned to the CH stretching vibrations, have not been included in this table. The assignment of the bands to a specific conformer was supported by the spectral changes induced by the NIR irradiations. Some bands ascribed to the *trans* conformer were only experimentally detected upon the NIR irradiations at 6970 cm^{-1}. [b] Calculated harmonic wavenumbers were multiplied by 0.950 (above 3200 cm^{-1}) or 0.980 (below 3200 cm^{-1}). Wavenumbers in cm^{-1}. [c] Abbreviations: ν = stretching, δ = in-plane bending, γ = out-of-plane bending, τ = torsion, s = symmetric, and as = antisymmetric. Definition of internal coordinates and potential energy distribution for the *cis* and *trans* conformers of 2CP are given as supporting information (see Tables S2, S4 and S5).

TOG Graphic
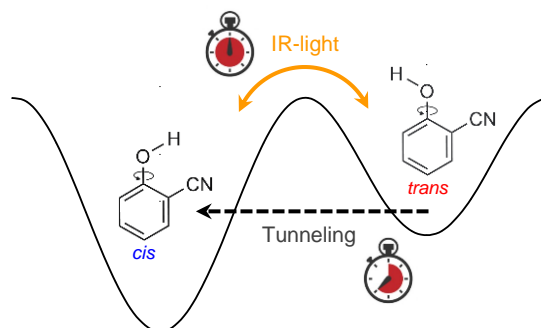
SUPPORTING INFORMATION

The Effects of Entangled IR-Radiation and Tunneling on the Conformational Interconversion of 2-Cyanophenol

A. J. Lopes Jesus,[a,b,*] Cláudio M. Nunes,[a] I. Reva,[a] Sandra M. V. Pinto,[a,c] and R. Fausto[a]

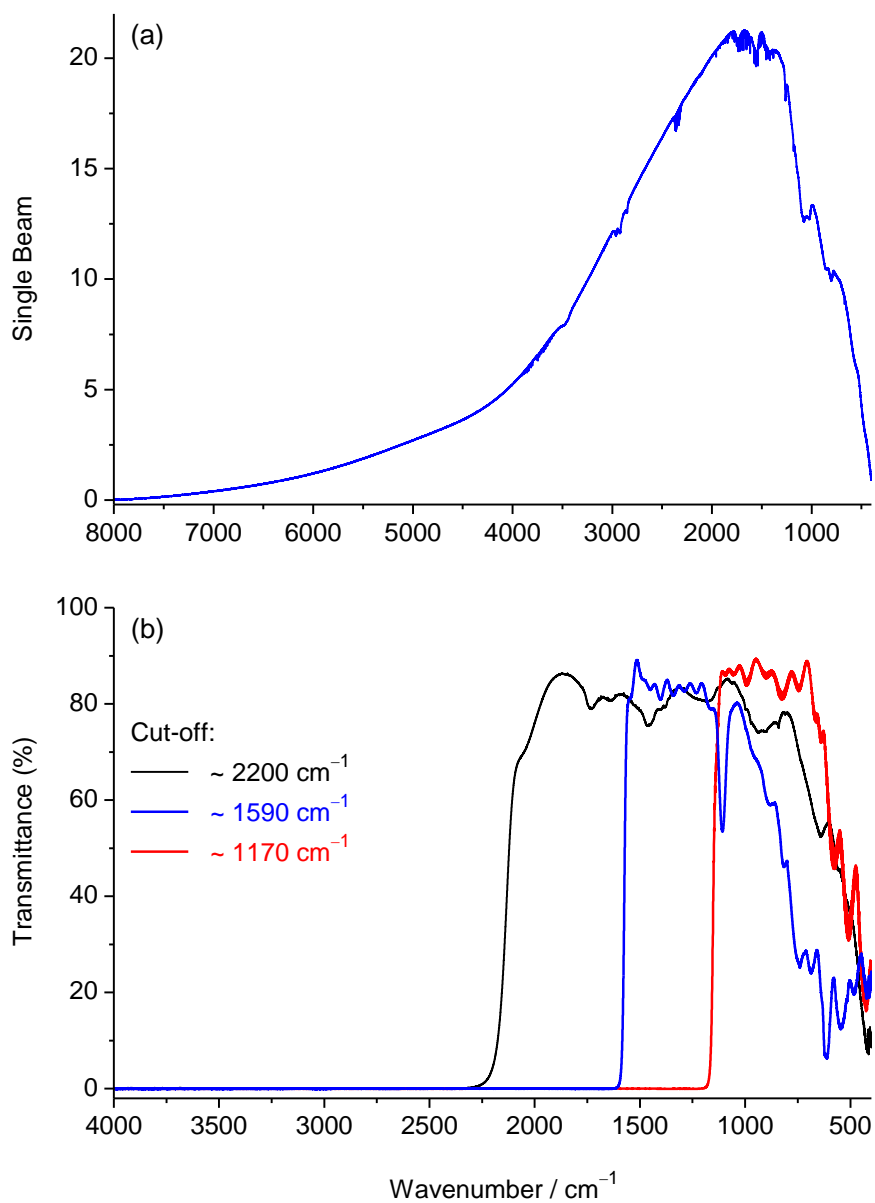[a] CQC, Department of Chemistry, University of Coimbra, 3004-535, Coimbra, Portugal.
[b] CQC, Faculty of Pharmacy, University of Coimbra, 3004-295, Coimbra, Portugal.
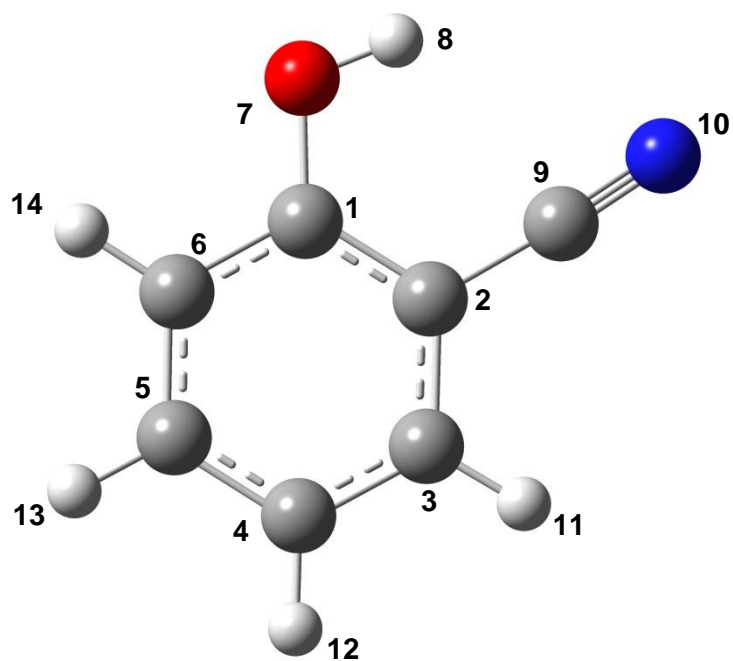[c] Scuola Normale Superiore, Piazza dei Cavalieri, 7, I-56124 Pisa, Italy.

* Corresponding author: A.J. Lopes Jesus

E-mail: ajorge@ff.uc.pt

Figure S1. Top: Single beam spectrum recorded with a ETC EverGlo IR source. Bottom: Transmittance spectra of the longpass filters used in the present work.

Figure S2. Atom numbering of 2-cyanophenol (2CP) used in this work. See the Cartesian coordinates in Table S1 and the definition of internal coordinates in Table S2.
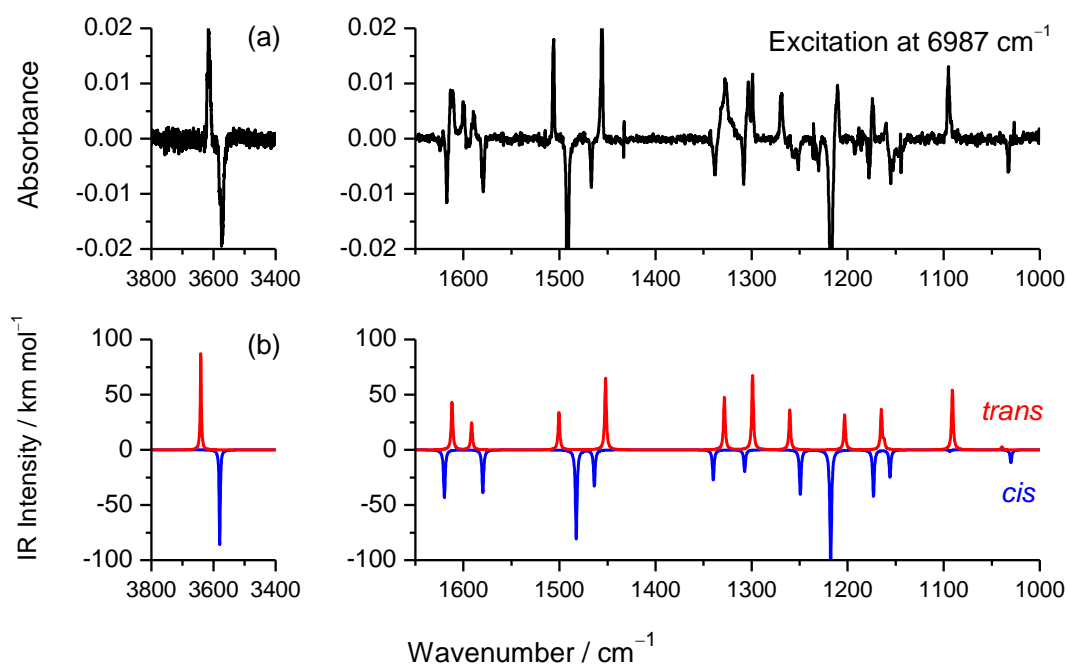
Figure S3. (a) Spectral changes observed after irradiating monomers of 2CP isolated in an N_2 matrix (15 K) with NIR laser-light tuned at 6987 cm^{-1}, wavenumber that corresponds to the position of one of the minor components of the 2v(OH) multiplet assigned to the *cis* form. These changes are represented as a difference spectrum which was obtained by subtracting the spectrum recorded before the irradiation from that recorded after the irradiation at 6987 cm^{-1} (upward bands are those growing upon the NIR irradiation). These changes are compared with the **(b)** spectra simulated for the *trans* (red trace, positive bands) and *cis* (blue trace, negative bands) conformers of 2CP by using the results of the B3LYP/6-311++G(d,p) harmonic vibrational calculations (details of the spectral simulations are given in the computational section of the manuscript). Identical changes were observed by tuning the laser at 6961 cm^{-1}, which corresponds to the position of a shoulder found within 2v(OH) band profile ascribed to the *cis* conformer.
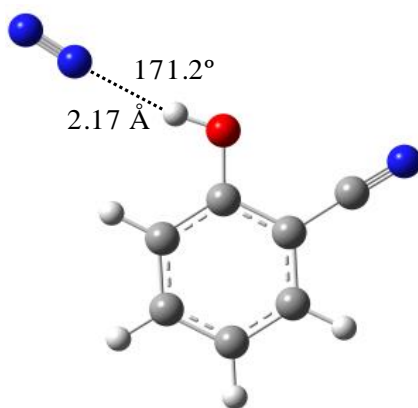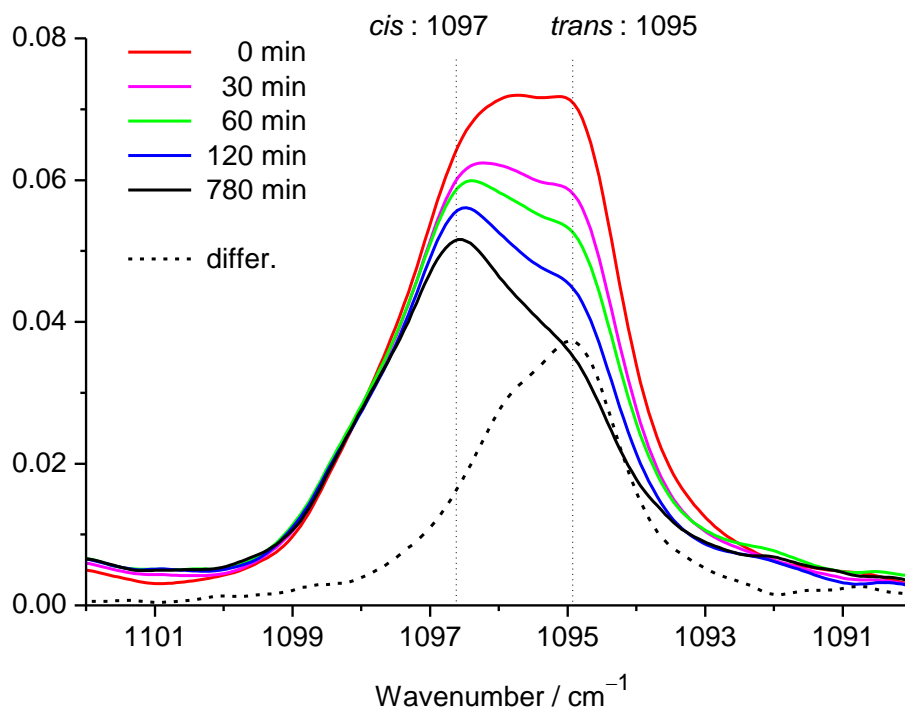
trans···N₂, ΔE_{bind} = -8.54 kJ mol^{-1}
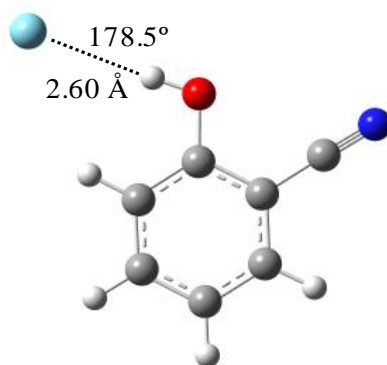
trans···Ar, ΔE_{bind} = -2.93 kJ mol^{-1}

Figure S4. MP2/6-311++G(3df,3pd) optimized geometries of the OH-bound complexes of *trans*-2CP with a nitrogen (N₂) molecule and an argon (Ar) atom, including the BSSE (basis set superposition error) corrected binding energies (ΔE_{bind}) and some geometrical parameters: H···X distance and O–H···X angle (X = N₂ or Ar).

Figure S5. Fragment of IR spectra of 2CP isolated in an N_2 matrix at 15 K, recorded during the permanence of the sample in the dark. Before the registration of the first spectrum (0 min), the sample was enriched with the *trans* form by performing NIR irradiations at 6970 cm^{-1}. Each spectrum was recorded in the presence of a cutoff filter transmitting only below 1170 cm^{-1}. Vertical dotted lines indicate the positions of the band components assigned to the *cis* and *trans* conformers of 2CP. In this figure is also shown a difference spectrum (dashed line) obtained by subtracting the black spectrum (recorded after letting the sample in dark for 780 min) from the red spectrum (recorded at the beginning of the "dark" kinetics).

Table S1. Cartesian Coordinates (Å) for the *cis* and *trans* conformers of 2-cyanophenol (2CP) optimized at different levels of theory

B3LYP/6-311++G(d,p)

		cis			*trans*	
C	-0.655536	-0.623266	0.000000	-0.697297	-0.597537	0.000000
C	0.000000	0.625257	0.000000	0.000000	0.625384	0.000000
C	1.404173	0.680280	0.000000	1.402904	0.618988	0.000000
C	2.147425	-0.488684	0.000000	2.106594	-0.577866	0.000000
C	1.489185	-1.723469	0.000000	1.406782	-1.784865	0.000000
C	0.103106	-1.795237	0.000000	0.015813	-1.797265	0.000000
O	-2.004375	-0.743878	0.000000	-2.053184	-0.544780	0.000000
H	-2.427493	0.125706	0.000000	-2.421939	-1.434694	0.000000
C	-0.793689	1.809393	0.000000	-0.712362	1.863136	0.000000
N	-1.496541	2.728989	0.000000	-1.260669	2.880273	0.000000
H	1.889719	1.648311	0.000000	1.926072	1.567226	0.000000
H	3.229220	-0.444142	0.000000	3.189280	-0.571140	0.000000
H	2.066097	-2.641204	0.000000	1.945511	-2.725400	0.000000
H	-0.414746	-2.746213	0.000000	-0.523371	-2.739511	0.000000

MP2/6-311++G(3df,3pd)

		cis			*trans*	
C	-0.637703	-0.628922	0.000000	-0.685131	-0.604076	0.000000
C	0.000000	0.622029	0.000000	0.000000	0.619001	0.000000
C	1.397696	0.707064	0.000000	1.399025	0.634908	0.000000
C	2.158196	-0.452867	0.000000	2.113563	-0.556050	0.000000
C	1.522627	-1.695880	0.000000	1.428884	-1.769535	0.000000
C	0.136676	-1.786951	0.000000	0.037953	-1.794476	0.000000
O	-1.984598	-0.763751	0.000000	-2.040769	-0.552665	0.000000
H	-2.400419	0.107892	0.000000	-2.392004	-1.448118	0.000000
C	-0.823835	1.785763	0.000000	-0.735796	1.842720	0.000000
N	-1.584350	2.679299	0.000000	-1.316833	2.860741	0.000000
H	1.863893	1.682874	0.000000	1.907383	1.589504	0.000000
H	3.237088	-0.390061	0.000000	3.194110	-0.537466	0.000000
H	2.111451	-2.603352	0.000000	1.975379	-2.703049	0.000000
H	-0.366722	-2.743865	0.000000	-0.491877	-2.739691	0.000000

QCISD/6-31++G(d,p)

		cis			*trans*	
C	-0.647729	-0.627336	0.000000	-0.685720	-0.607421	0.000000
C	0.000000	0.619972	0.000000	0.000000	0.619022	0.000000
C	1.405974	0.690235	0.000000	1.403755	0.634902	0.000000
C	2.159012	-0.478139	0.000000	2.122272	-0.560052	0.000000
C	1.505506	-1.721293	0.000000	1.432033	-1.777285	0.000000
C	0.115675	-1.801465	0.000000	0.035832	-1.805511	0.000000
O	-2.006360	-0.761395	0.000000	-2.052248	-0.558167	0.000000
H	-2.433330	0.106448	0.000000	-2.411406	-1.453398	0.000000
C	-0.809900	1.813188	0.000000	-0.739740	1.859332	0.000000
N	-1.528545	2.738238	0.000000	-1.312404	2.879760	0.000000
H	1.883153	1.661719	0.000000	1.915423	1.588627	0.000000
H	3.239414	-0.427391	0.000000	3.203723	-0.543034	0.000000
H	2.087307	-2.634474	0.000000	1.979641	-2.711329	0.000000
H	-0.397076	-2.753779	0.000000	-0.493157	-2.751783	0.000000

Table S2. Definition of internal coordinates used in the normal mode analysis of 2CP[a]

Coordinate	Definition	Approximate description
S_1	$r_{7,8}$	$\nu(OH)$
S_2	$(4^{-1/2})\,(r_{3,11} + r_{4,12} + r_{5,13} + r_{6,14})$	$\nu_1(CH)_s$
S_3	$(4^{-1/2})\,(r_{3,11} + r_{4,12} - r_{5,13} - r_{6,14})$	$\nu_2(CH)_{as}$
S_4	$(4^{-1/2})\,(r_{3,11} - r_{4,12} + r_{5,13} - r_{6,14})$	$\nu_3(CH)_{as}$
S_5	$(4^{-1/2})\,(r_{3,11} - r_{4,12} - r_{5,13} + r_{6,14})$	$\nu_4(CH)_{as}$
S_6	$r_{2,9}$	$\nu(CC)_{CN}$
S_7	$r_{9,10}$	$\nu(CN)$
S_8	$r_{1,7}$	$\nu(CO)$
S_9	$(2^{-1/2})\,(r_{1,2} + r_{4,5})$	$\nu_1(CC)_s$
S_{10}	$(2^{-1/2})\,(r_{1,2} - r_{4,5})$	$\nu_1(CC)_{as}$
S_{11}	$(2^{-1/2})\,(r_{2,3} + r_{5,6})$	$\nu_2(CC)_s$
S_{12}	$(2^{-1/2})\,(r_{2,3} - r_{5,6})$	$\nu_2(CC)_{as}$
S_{13}	$(2^{-1/2})\,(r_{1,6} + r_{3,4})$	$\nu_3(CC)_s$
S_{14}	$(2^{-1/2})\,(r_{1,6} - r_{3,4})$	$\nu_3(CC)_{as}$
S_{15}	$(4^{-1/2})\,(\beta_{11,2,3} - \beta_{11,4,3} + \beta_{14,5,6} - \beta_{14,1,6})$	$\delta_1(CH)_s$
S_{16}	$(4^{-1/2})\,(\beta_{11,2,3} - \beta_{11,4,3} - \beta_{14,5,6} + \beta_{14,1,6})$	$\delta_1(CH)_{as}$
S_{17}	$(4^{-1/2})\,(\beta_{11,2,3} - \beta_{11,4,3} + \beta_{14,5,6} - \beta_{14,1,6})$	$\delta_2(CH)_s$
S_{18}	$(4^{-1/2})\,(\beta_{11,2,3} - \beta_{11,4,3} - \beta_{14,5,6} + \beta_{14,1,6})$	$\delta_2(CH)_{as}$
S_{19}	$(6^{-1/2})\,(\beta_{1,3,2} - \beta_{2,4,3} + \beta_{3,5,4} - \beta_{4,6,5} + \beta_{5,1,6} - \beta_{6,2,1})$	$\delta(ring)$
S_{20}	$(8^{-1/2})\,(-\beta_{1,3,2} - \beta_{2,4,3} + 2\beta_{3,5,4} - \beta_{4,6,5} - \beta_{5,1,6} + 2\beta_{6,2,1})$	$\delta(ring)_{as}$
S_{21}	$(4^{-1/2})\,(\beta_{1,3,2} - \beta_{2,4,3} + \beta_{4,6,5} - \beta_{5,1,6})$	$\delta(ring)_{as'}$
S_{22}	$(2^{-1/2})\,(\beta_{9,1,2} - \beta_{9,3,2})$	$\delta(CC)_{CN}$
S_{23}	$(2^{-1/2})\,(\beta_{7,6,1} - \beta_{7,2,1})$	$\delta(CO)$
S_{24}	$\beta_{8,1,7}$	$\delta(COH)$
S_{25}	$\beta_{9,3,10,2}$	$\delta(CCN)$
S_{26}	$\gamma_{9,3,10,2}$	$\gamma(CCN)$
S_{27}	$(6^{-1/2})\,(\tau_{1,2,3,4} - \tau_{2,3,4,5} + \tau_{3,4,5,6} - \tau_{4,5,6,1} + \tau_{5,6,1,2} - \tau_{6,1,2,3})$	$\tau(ring)$
S_{28}	$(8^{-1/2})\,(2\tau_{1,2,3,4} - \tau_{2,3,4,5} - \tau_{3,4,5,6} + 2\tau_{4,5,6,1} - \tau_{5,6,1,2} - \tau_{6,1,2,3})$	$\tau(ring)_{as}$
S_{29}	$(4^{-1/2})\,(\tau_{2,3,4,5} - \tau_{3,4,5,6} + \tau_{5,6,1,2} - \tau_{6,1,2,3})$	$\tau(ring)_{as'}$
S_{30}	$\tau_{8,7,1,2}$	$\tau(COH)$
S_{31}	$(4^{-1/2})\,(\gamma_{11,2,3,4} - \gamma_{11,2,3,4} + \gamma_{12,3,4,5} - \gamma_{12,3,4,5})$	$\gamma_1(CH)_s$
S_{32}	$(4^{-1/2})\,(\gamma_{11,2,3,4} - \gamma_{11,2,3,4} - \gamma_{12,3,4,5} + \gamma_{12,3,4,5})$	$\gamma_1(CH)_{as}$
S_{33}	$(4^{-1/2})\,(\gamma_{13,4,5,6} - \gamma_{13,4,5,6} + \gamma_{14,5,6,1} - \gamma_{14,5,6,1})$	$\gamma_2(CH)_s$
S_{34}	$(4^{-1/2})\,(\gamma_{13,4,5,6} - \gamma_{13,4,5,6} - \gamma_{14,5,6,1} + \gamma_{14,5,6,1})$	$\gamma_2(CH)_{as}$
S_{35}	$(4^{-1/2})\,(\gamma_{7,6,1,2} - \gamma_{7,6,1,2} + \gamma_{9,1,2,3} - \gamma_{9,1,2,3})$	$\gamma(CO) + \gamma(CC)_{CN}$
S_{36}	$(4^{-1/2})\,(\gamma_{7,6,1,2} - \gamma_{7,6,1,2} - \gamma_{9,1,2,3} + \gamma_{9,1,2,3})$	$\gamma(CO) - \gamma(CC)_{CN}$

[a] Abbreviations: ν − stretching, δ – in-plane bending, γ − out-of-plane bending, τ – torsion. See Figure S1 for atom numbering; $r_{i,j}$ is the distance between atoms A_i and A_j; $\beta_{i,j,k}$ is the angle between vectors A_kA_i and A_kA_j; $\beta_{i,j,k,l}$ is the angle between vector A_kA_i and A_kA_j in the plane defined by A_i, A_k, A_l atoms; $\tau_{i,j,k,l}$ is the dihedral angle between the plane defined by A_i, A_j, A_k and the plane defined by A_j, A_k, A_l atoms; $\gamma_{i,j,k,l}$ is the angle between the vector A_kA_i and the plane defined by atoms A_j, A_k, A_l. The combinations [(+), (+)] and [(+), (−)] denote in-phase and in-opposite-phase couplings between coordinates of different types.

Table S3. Overtone transitions for the *cis* and *trans* conformers of 2CP [E = vibrational energy, cm^{-1}; I = infrared intensity, km mol^{-1}] obtained by means of anharmonic vibrational calculations carried out at the B3LYP/6-31++G(d,p) level of theory.

Mode (Quanta)	*cis*			*trans*		
	E (harm)	E (anharm)	I (anharm)	E (harm)	E (anharm)	I (anharm)
1(2)	**7523.982**	**6965.800**	**3.907**	**7650.843**	**7105.793**	**5.722**
2(2)	6443.939	6157.216	0.102	6441.699	6130.960	0.385
3(2)	6434.941	6118.292	0.130	6416.427	6108.096	0.509
4(2)	6412.738	6107.894	0.597	6394.440	6094.189	1.005
5(2)	6387.077	6044.191	1.338	6350.383	5993.276	1.033
6(2)	4635.257	4543.728	0.173	4672.722	4580.613	0.110
7(2)	3320.772	3235.761	0.125	3304.137	3220.728	0.025
8(2)	3239.629	3167.472	1.606	3263.469	3187.019	1.416
9(2)	3037.769	2968.514	0.085	3073.119	2998.640	0.083
10(2)	2996.380	2924.351	0.056	2972.279	2904.468	0.010
11(2)	2747.348	2673.464	0.303	2730.393	2665.175	0.610
12(2)	2681.567	2621.235	0.225	2658.269	2596.655	0.568
13(2)	2561.455	2509.506	0.659	2586.535	2527.920	0.338
14(2)	2487.533	2436.146	1.469	2455.561	2419.752	0.856
15(2)	2394.908	2358.420	0.254	2376.476	2345.082	0.124
16(2)	2362.997	2336.631	0.037	2373.234	2335.445	0.405
17(2)	2232.369	2196.250	0.002	2225.828	2187.880	0.086
18(2)	2106.662	2071.143	0.057	2125.570	2087.202	0.038
19(2)	1713.844	1687.113	0.205	1710.163	1688.423	0.174
20(2)	1480.088	1458.062	2.479	1479.380	1456.479	0.591
21(2)	1208.241	1193.284	11.486	1204.942	1189.926	3.561
22(2)	1131.262	1120.672	0.106	1124.352	1114.875	2.510
23(2)	937.494	929.149	0.048	932.413	922.417	0.040
24(2)	776.134	771.223	0.005	744.683	738.821	0.096
25(2)	275.411	278.873	0.028	299.436	299.066	0.026
26(2)	1995.672	1961.167	1.981	1980.593	1955.123	2.206
27(2)	1927.134	1891.011	0.941	1917.336	1884.419	0.724
28(2)	1747.526	1756.944	0.226	1720.550	1714.333	0.575
29(2)	1542.614	1518.100	0.494	1530.691	1507.715	0.545
30(2)	1430.004	1838.749	2.067	1463.427	1607.748	0.238
31(2)	1153.873	1149.759	0.107	1165.400	1151.196	0.118
32(2)	1010.259	1002.849	0.394	1013.110	989.921	0.147
33(2)	882.928	817.126	6.493	798.968	787.172	0.005
34(2)	797.494	805.355	0.195	698.611	643.498	10.093
35(2)	469.641	475.512	0.066	471.907	469.164	0.197
36(2)	264.017	267.129	0.003	255.712	250.206	0.014

Bold wavenumbers and intensities refer to the computed OH stretching overtones (2νOH)

Table S4. B3LYP/6-311++G(d,p) calculated harmonic wavenumbers ($\tilde{\nu}$ / cm^{-1}), absolute IR intensities (I) and potential energy distributions (PED) for the *cis* conformer of 2CP

$\tilde{\nu}$ / cm$^{-1\,a}$	I / km mol^{-1}	Sym.	PED (%)^{b}
3580.0	85.9	A'	100.0 (S_1)
3141.2	3.9	A'	95.8 (S_2)
3136.3	4.2	A'	78.9 (S_3) ; 13.3 (S_4)
3126.1	3.2	A'	86.6 (S_5) ; 11.5 (S_4)
3112.9	2.5	A'	73.7 (S_4) ; 16.8 (S_3)
2268.7	64.7	A'	89.2 (S_7) ; 10.8 (S_6) ;
1619.8	43.3	A'	43.8 (S_{13}) ; 19.5 (S_{11}) ; 11.7 (S_{15})
1579.8	38.8	A'	39.7 (S_9) ; 25.0 (S_{11}) ; 10.8 (S_{18})
1482.5	81.0	A'	39.9 (S_{16}) ; 21.4 (S_{10}) ; 10.7 (S_{12}) ; 9.9 (S_{18})
1463.7	32.8	A'	40.7 (S_{17}) ; 22.7 (S_{14}) ; 12.9 (S_{12})
1339.9	27.5	A'	33.7 (S_{24}) ; 14.8 (S_{14}) ; 13.8 (S_{15}) ; 10.7 (S_{10}) ; 9.7 (S_{17})
1307.3	19.8	A'	19.3 (S_8) ; 19.3 (S_{12}) ; 14.9 (S_{15}) ; 13.7 (S_{10}) ; 12.1 (S_{17})
1249.3	40.5	A'	23.9 (S_8) ; 22.7 (S_{11}) ; 19.7 (S_{15}) ; 9.6 (S_{12})
1217.7	109.1	A'	28.4 (S_{24}) ; 18.9 (S_6) ; 15.4 (S_{19}) ; 9.5 (S_{14}) ;
1173.1	42.1	A'	23.5 (S_{13}) ; 22.7 (S_{18}) ; 21.0 (S_{15}) ; 13.4 (S_{24})
1155.9	24.7	A'	39.7 (S_{18}) ; 24.9 (S_{16})
1093.5	1.5	A'	26.3 (S_{14}) ; 21.8 (S_{19}) ; 17.1 (S_{17})
1030.0	11.6	A'	30.8 (S_{10}) ; 19.1 (S_{16}) ; 15.2 (S_9)
971.1	0.1	A"	76.2 (S_{34}) ; 34.3 (S_{32})
943.6	2.1	A"	79.0 (S_{32}) ; 28.7 (S_{34})
853.5	0.7	A"	48.5 (S_{33}) ; 36.6 (S_{31}) ; 12.1 (S_{34}) ; 10.7 (S_{36})
840.6	10.9	A'	45.9 (S_{19}) ; 19.2 (S_8) ; 11.8 (S_{20})
755.1	67.9	A"	50.2 (S_{31}) ; 37.8 (S_{33})
724.4	9.0	A'	25.5 (S_{21}) ; 20.0 (S_9) ; 19.2 (S_6)
707.2	0.8	A"	62.8 (S_{27}) ; 44.3 (S_{36})
600.4	0.3	A'	41.3 (S_{22}) ; 20.8 (S_{25}) ; 15.8 (S_{20})
569.8	2.6	A"	37.9 (S_{27}) ; 25.6 (S_{36}) ; 23.5 (S_{26}) ; 9.8 (S_{29})
556.7	5.3	A'	31.6 (S_{21}) ; 20.3 (S_{20}) ; 13.3 (S_{23})
494.5	10.7	A"	42.1 (S_{35}) ; 24.6 (S_{29}) ; 11.1 (S_{26})
464.2	0.1	A'	34.9 (S_{20}) ; 18.2 (S_{23}) ; 10.5 (S_{25})
412.0	109.3	A"	79.9 (S_{30}) ; 17.9 (S_{28})
391.0	4.0	A"	69.4 (S_{28}) ; 25.6 (S_{26}) ; 18.7 (S_{30})
381.8	4.0	A'	47.3 (S_{23}) ; 20.6 (S_{21})
229.5	0.0	A"	55.3 (S_{29}) ; 36.2 (S_{35}) ; 12.1 (S_{26})
138.2	7.2	A'	57.0 (S_{25}) ; 37.7 (S_{22})
128.8	2.7	A"	23.7 (S_{29}) ; 23.3 (S_{26}) ; 23.2 (S_{36}) ; 15.0 (S_{28})

^{a} Calculated harmonic wavenumbers were multiplied by 0.95 (above 3300 cm^{-1}) or 0.98 (below 3300 cm^{-1}). ^{b} See Table S2 for the definition of internal coordinates; PED values lower than 10% are not included.

Table S5. B3LYP/6-311++G(d,p) calculated wavenumbers ($\tilde{v}$ / cm^{-1}), absolute IR intensities (I) and potential energy distributions (PED) for the *trans* conformer of 2CP

$\tilde{v}$ / cm$^{-1\,a}$	I / km mol^{-1}	Symmetry	PED (%) [b]
3641.0	87.2	A'	100.0 (S$_1$)
3140.4	4.9	A'	71.7 (S$_2$) ; 25.2 (S$_3$)
3127.9	4.8	A'	60.5 (S$_5$) ; 21.9 (S$_3$) ; 13.8 (S$_4$)
3117.3	3.8	A'	43.8 (S$_3$) ; 38.9 (S$_4$) ; 13.4 (S$_2$)
3096.1	8.0	A'	46.6 (S$_4$) ; 33.8 (S$_5$) ; 10.8 (S$_2$)
2287.0	39.4	A'	89.1(S$_7$) ; 11.0 (S$_6$)
1611.9	43.4	A'	44.4 (S$_{13}$) ; 14.5 (S$_{11}$) ; 11.4 (S$_{15}$)
1591.5	24.7	A'	38.3 (S$_9$) ; 28.6 (S$_{11}$)
1500.6	33.9	A'	36.6 (S$_{16}$) ; 22.4 (S$_{10}$) ; 11.8 (S$_{18}$)
1452.0	65.1	A'	49.0 (S$_{17}$) ; 19.6 (S$_{14}$) ; 14.1 (S$_{12}$)
1328.4	47.6	A'	25.6 (S$_{14}$) ; 22.7 (S$_{24}$) ; 13.1 (S$_{10}$) ; 11.4 (S$_{15}$) ; 11.1(S$_{12}$)
1299.0	67.3	A'	30.8 (S$_{15}$) ; 19.4 (S$_8$) ; 15.5 (S$_{12}$) ; 10.2 (S$_{17}$)
1260.3	36.2	A'	30.0 (S$_8$) ; 19.1 (S$_{11}$)
1203.2	31.9	A'	31.8 (S$_6$) ; 20.8 (S$_{24}$) ; 12.8 (S$_{19}$)
1164.9	36.2	A'	23.9 (S$_{24}$) ; 22.9 (S$_{15}$) ; 17.8 (S$_{18}$) ; 17.0 (S$_{13}$) ; 9.5 (S$_{17}$)
1162.0	6.4	A'	44.2 (S$_{18}$) ; 20.5 (S$_{16}$)
1091.0	54.0	A'	25.6 (S$_{14}$) ; 22.6 (S$_{19}$) ; 15.8 (S$_{17}$) ; 11.4 (S$_{24}$)
1039.3	2.7	A'	28.6 (S$_{10}$) ; 17.9 (S$_{16}$) ; 15.8 (S$_9$)
962.4	0.1	A"	91.8 (S$_{32}$) ; 22.7 (S$_{34}$)
933.9	1.6	A"	65.7 (S$_{34}$) ; 23.0 (S$_{32}$) ; 14.8 (S$_{31}$)
839.2	22.2	A'	45.7 (S$_{19}$) ; 19.6 (S$_8$) ; 12.8 (S$_{20}$)
835.9	0.2	A"	36.1(S$_{33}$) ; 34.2 (S$_{31}$) ; 29.1(S$_{34}$) ; 11.8 (S$_{36}$)
747.0	80.0	A"	50.6 (S$_{31}$) ; 34.8 (S$_{33}$) ; 16.2 (S$_{36}$)
724.3	2.7	A'	26.9 (S$_{21}$) ; 19.0 (S$_6$) ; 18.8 (S$_9$) ; 9.7 (S$_{11}$)
717.9	0.3	A"	49.9 (S$_{27}$) ; 48.6 (S$_{36}$) ; 13.4 (S$_{33}$)
597.7	2.6	A'	51.9 (S$_{22}$) ; 12.4 (S$_{20}$) ; 12.0 (S$_{25}$)
572.3	0.8	A"	57.3 (S$_{27}$) ; 31.4 (S$_{36}$) ; 22.4 (S$_{35}$) ; 10.0 (S$_{26}$)
554.0	0.8	A'	30.7 (S$_{21}$) ; 20.1 (S$_{20}$) ; 13.4 (S$_{23}$)
495.7	11.4	A"	48.8 (S$_{35}$) ; 40.4 (S$_{29}$) 10.1(S$_{26}$)
460.6	4.6	A'	42.4 (S$_{20}$) ; 11.8 (S$_{23}$) ; 10.5 (S$_6$)
390.2	0.1	A"	121.2 (S$_{28}$)
366.8	8.5	A'	55.6 (S$_{23}$) ; 19.9 (S$_{21}$)
319.6	112.1	A"	94.5 (S$_{30}$)
229.7	0.3	A"	64.2 (S$_{29}$) ; 27.7 (S$_{35}$) ; 11.6 (S$_{27}$) ; 11.3(S$_{26}$)
149.8	2.4	A'	76.0 (S$_{25}$) ; 21.3 (S$_{22}$)
125.1	0.0	A"	58.9 (S$_{26}$) ; 15.6 (S$_{29}$) ; 10.5 (S$_{36}$)

[a] Calculated harmonic wavenumbers were multiplied by 0.95 (above 3300 cm^{-1}) or 0.98 (below 3300 cm^{-1}). [b] See Table S2 for the definition of internal coordinates; PED values lower than 10% are not included.